Identifying Robust Decarbonization Pathways for the Western U.S. Electric Power System under Deep Climate Uncertainty

Srihari Sundar[1], Flavio Lehner[2,3,4], Nathalie Voisin[5,6] and Michael T. Craig[7,8*]

[1]Department of Aerospace Engineering, University of Michigan, Ann Arbor, Michigan, USA.
[2]Department of Earth and Atmospheric Sciences, Cornell University, Ithaca, NY, USA.
[3]Climate and Global Dynamics Laboratory, National Center for Atmospheric Research, Boulder, CO, USA.
[4]Polar Bears International, Bozeman, MT, USA.
[5]Pacific Northwest National Laboratory, Richland, WA, USA.
[6]University of Washington, Seattle, WA, USA.
[7]School for Environment and Sustainability, University of Michigan, Ann Arbor, Michigan, USA.
[8]Department of Industrial and Operations Engineering, University of Michigan, Ann Arbor, Michigan, USA.

*Corresponding author(s). E-mail(s): mtcraig@umich.edu;

Abstract

Climate change threatens the resource adequacy of future power systems. Existing research and practice lack frameworks for identifying decarbonization pathways that are robust to climate-related uncertainty. We create such an analytical framework, then use it to assess the robustness of alternative pathways to achieving 60% emissions reductions from 2022 levels by 2040 for the Western U.S. power system. Our framework integrates power system planning and resource adequacy models with 100 climate realizations from a large climate ensemble. Climate realizations drive electricity demand; thermal plant availability; and wind, solar, and hydropower generation. Among five initial decarbonization pathways, all exhibit modest to significant resource adequacy failures under climate realizations in 2040, but certain pathways experience significantly less resource adequacy failures at little additional cost relative to other pathways. By identifying and planning for an extreme climate realization that drives the largest resource adequacy failures across our pathways, we produce a new decarbonization pathway that has no resource adequacy failures under any climate realizations. Our framework can help planners adapt to climate change, and offers a unique bridge between energy system and climate modelling.

Keywords: robust decision-making, climate adaptation, capacity expansion, single model initial condition large ensemble, power system decarbonization

1 Introduction

Rapidly transitioning to a decarbonized electric power sector is crucial to aggressively mitigate climate change and meet emissions reductions targets [1, 2]. In the United States, the Inflation Reduction Act (IRA) is poised to accelerate low-carbon investments in the power sector, which could approach 370 billion USD by 2033 [3, 4]. Which power sector decarbonization pathway will be taken remains uncertain, where a pathway is defined by where, when, and what decarbonization investments occur [5–11]. As they decarbonize, bulk (or tranmission-scale) power systems will be increasingly affected by climate change [12]. Increasing ambient air temperatures will increase peak and total electricity demand [13–15] and reduce available capacity from thermal and solar generators [13, 16–18]. Wind, solar, and precipitation changes will also affect wind, solar, and hydropower generation potential [13, 19–21]. These effects could compound to undermine resource adequacy (RA), or a system's ability to continually balance electricity supply and demand [22–24]. Understanding the vulnerability of decarbonizing power systems to potential future climate realizations is critical for achieving reliable, affordable, and clean power systems - the focus of our study [9, 25].

To account for decarbonization- and climate-related uncertainty in investment decisions, prior literature optimizes capacity investment decisions given different decarbonization pathways and future climate scenarios [5, 9, 26–32]. This literature uses sensitivity or scenario analysis to incorporate climate-related uncertainty within deterministic modeling frameworks. For instance, Fonseca et al. [5] sample 3 of 20 global climate models (GCMs) to include as scenarios in a deterministic long-term power system planning model. In other words, this literature aims to improve investment decisions by improving predictions of future weather within standard modeling frameworks. But climate change poses deep uncertainty [33], which undermines the value of methods focused on better predictions [34], particularly for power system planning models that must significantly simplify uncertainty to remain computationally tractable. In the near-term (prior to 2050), inter-annual (or internal) climate variability, which is driven by the dynamics of the climate system and sensitive to initial conditions [35–38], is the primary source of climate-related uncertainty [37, 39] (as opposed to model or emissions scenario uncertainty [40]). Inter-annual variability superimposed on a non-stationary background climate and emission trajectory leads to deep uncertainty on climate impacts [41]. Under deep uncertainty, methods instead focused on identifying robust strategies or alternatives are better suited to informing decisions [34]. Such decision support is urgently needed by power system planners and regulators, who are tasked with ensuring resource adequacy across the full range of potential future climate realizations, which combine secular trends and inter-annual climate variability [38]. Recent rolling outages in California and Texas [42, 43] and resource adequacy warnings elsewhere in the United States [44] underscore this urgency.

In response to these needs, we construct a new analytical framework for planning decarbonizing power systems under deep climate uncertainty by drawing on a concept from the decision science literature: robust decision making (RDM) [34]. RDM has been used to inform climate adaptation strategies, e.g. in water resources management [45–51]. It has also been used in the power sector, e.g. to evaluate policy strategies for European power systems against shocks [52]. But our framework is the first to apply RDM to planning decarbonizing power systems under deep climate uncertainty. By integrating power system planning and operational models with potential climate realizations from a single model initial-condition large ensemble (SMILE) [53, 54], our framework generates alternative decarbonization pathways; characterizes the vulnerability of and trade-offs between those pathways under potential climate realizations; and uses generated insights to identify new alternative decarbonization pathways that are robust to climate-related uncertainty (Figure 1). SMILEs have limited prior use in power systems research [55, 56] even though they are designed to sample inter-annual variability and provide many realizations of future climate, encoding multiple extreme events and a range of possible meteorological projections [57, 58].

We use our framework to answer: how can we design decarbonizing power systems to be robust against deep climate uncertainty? We conduct our study for the U.S. Western Interconnect, which we divide into five subregions per Western Electricity Coordinating Council's resource adequacy assessments (Figure E.1, [59]). We use 100 members from the Community Earth System Model 2 (CESM2) Large Ensemble (LENS2) through 2040, which was driven by the SSP3-7.0 emissions scenario and reaches 1.65°C of global warming by 2040 relative to pre-industrial [60]. For each ensemble member, we obtain surface air temperatures, relative humidity, surface solar radiation, 10m wind speeds, and surface runoff at daily and 1° spatial resolution (approx. 100 km by 100 km) through 2040 across our study region. While this resolution is lower than what is preferred for power system modeling, higher resolution climate datasets often do not sample as large of a range of internal climate variability as LENS2, particularly in the time-span of interest to us (through 2040) and when focused on extreme events. In selecting LENS2, we also emphasize internal variability over climate response uncertainty. For each ensemble member, we translate meteorological variables to spatially-explicit timeseries of electricity demand; maximum potential wind, solar, and hydropower generation; and thermal generator deratings and forced outage rates. To analyze the vulnerability and trade-offs of alternative decarbonization pathways, we generate five decarbonization pathways by running a capacity expansion (or long-term planning) model of the Western Interconnect using power system variables from five sampled ensemble members. Our decarbonization pathways reduce interconnect-wide power system CO_2 emissions by 60% from 2022 levels by 2040. For each decarbonization pathway, we approximate its regional resource adequacy in 2040 under each of the 100 ensemble members using economic dispatch and surplus available capacity models. From this large set of alternative future systems and climate realizations, we examine vulnerabilities and trade-offs of these decarbonization pathways across potential climate realizations. Finally, we identify a future climate realization that generates the largest resource adequacy failures across decarbonization pathways in 2040, then use that climate realization to generate a new decarbonization pathway robust to all 100 ensemble members.

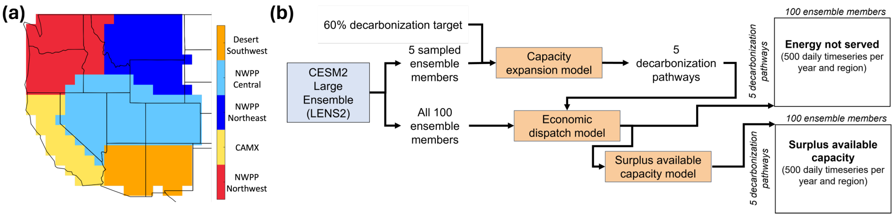

Fig. 1: (a) Map of our Western Interconnect study region, which is divided into 5 sub-regions (differentiated by color). Blocks at edges of interconnect correspond to LENS2 grid cells. (b) Our analytical framework integrates 100 ensemble members (or climate realizations) from the LENS2 dataset with power system capacity expansion, economic dispatch, and surplus available capacity (SAC) models. For each region, this framework yields 500 daily timeseries of energy not served and surplus available capacity in 2040, or 1 daily timeseries for each climate realization, decarbonization pathway, and metric. Not shown is identification of an extreme 2040 climate realization, which is then fed back into the capacity expansion model to generate a new decarbonization pathway.

2 Methods

2.1 Robust Decision-making Framework

We use robust decision-making (RDM) to quantify the robustness of alternative decarbonization pathways in the Western Interconnect power system to potential future climate realizations. We first conduct exploratory modeling to generate five decarbonization pathways for the Western Interconnect using a capacity expansion (or long-term planning) model (Section 2.2). We then stress test each decarbonization pathway to all 100 LENS2 ensemble members (Section 2.4). For each pathway and ensemble member, we approximate resource adequacy by quantifying daily Surplus Available Capacity (SAC) and Energy Not Served (ENS) in 2040 (Section 2.3). Finally, we identify the climate ensemble member that drives the largest combined energy not served (ENS) across decarbonization pathways in California (our largest load region) in 2040; rerun our planning model using that ensemble member; and quantify our resource adequacy metrics for that pathway against all 100 climate ensemble members.

2.2 Capacity Expansion Model and Decarbonization Pathways

To generate alternative decarbonization pathways, we use a capacity expansion (or long-term planning) model. We run the capacity expansion model (CEM) in two year increments from 2023 to 2040, capturing coincident, spatially-resolved meteorology and hydrology for each year (Section 2.4). The CEM is a deterministic linear program that minimizes fixed plus variable costs by deciding investment in wind plants, solar plants, and natural gas combined cycle (NGCC) plants with or without carbon capture and sequestration (CCS), and inter-regional transmission. These investment decisions differentiate our "decarbonization pathways". The CEM also optimizes operation of existing and new generators, and optimizes inter-regional transmission flows using the simplified transport method. All generator capacity investment decisions occur at the LENS2 grid cell level, i.e. on a 100 by 100 km grid across our study region, while transmission investments occur at inter-regional levels. We constrain thermal plant investments to grid cells that already contain large thermal units. Given the immature state of CCS technology, we allow the CEM to invest in NGCC or coal with CCS beginning in 2031. While we recognize the important role of grid-scale storage in decarbonizing power systems, our climate data is only available at daily resolution (Section 2.4). As such, we cannot model intra-day storage.

The CEM includes numerous system- and generator-level constraints. At the system level, the CEM balances regional supply (generation plus imports minus exports) and demand each day. To approximate system reliability standards, the CEM includes a 13% planning reserve margin, which requires derated capacity to exceed peak demand by at least 13%. Derated capacity accounts for wind and solar generation potential; a fixed 5% forced outage rate for wind and solar generators; temperature-dependent FORs for thermal and hydropower plants; and weather-driven deratings of combustion turbine, combined cycle, and coal-fired plants. At the generator level, wind and solar generation is limited by daily, spatially-specific wind and solar capacity factors (Section 2.4); hydropower generation is constrained by subregional monthly total generation; and generation from combustion turbine, combined cycle, and coal-fired plants is limited by daily, spatially-specific meteorology.

With the CEM, we generate five decarbonization pathways that each reduce interconnect-wide CO_2 emissions by 60% from 2022 levels by 2040. To create these five pathways, we use meteorological timeseries from five sampled LENS2 members. These ensemble members are sampled to capture a range of warming within the LENS2 ensemble. Specifically, we quantify warming level based on the difference between historic (1985-2015) and mid-century (2035-2065) mean surface temperature and relative humidity [61]. Warming and relative humidity levels vary from 1.5 °C to 2.75 °C and 0.1 to -1.79, respectively, across sampled ensemble members (Figure B.10). In using five sampled ensemble members, our purpose is to create heterogeneous decarbonization pathways that could all reach a given decarbonization target, then assess the pathways' vulnerabilities, trade-offs, and robustness. We do not create a pathway for each ensemble member because creating pathways that span all climate- and decarbonization-related uncertainty is not computationally tractable. Rather, researchers and practitioners explore a subset of this uncertainty in analyses and long-term plans. We therefore demonstrate our framework in a similar context, i.e. on pathways that consider a subset of relevant uncertainty.

2.3 Decarbonization Pathways and Resource Adequacy under Potential Climate Realizations

From our CEM, we obtain five decarbonization pathways, each planned for one of five sampled ensemble members. To understand the vulnerability of each decarbonization pathway to other potential ensemble members, we approximate the resource adequacy of each decarbonization pathway against all 100 ensemble members (or climate realizations) from LENS2. Because LENS2 provides daily values, we are unable to quantify resource adequacy (RA) of the Western Interconnect at an hourly basis using a standard probabilistic RA model. Instead, we approximate resource adequacy by quantifying daily Surplus Available Capacity (SAC) and Energy Not Served (ENS).

To calculate daily ENS, we run an economic dispatch model (EDM) for each decarbonization pathway output by our capacity expansion model in 2040. The EDM minimizes the sum of operating, CO_2 emission, inter-regional transmission, and ENS costs by optimizing generation, inter-regional transmission, and ENS decision variables. CO_2 emission costs include a decarbonization-pathway-specific CO_2 price necessary to achieve the relevant CO_2 emissions cap in that year; we include this price instead of a cap to avoid infeasibility in the EDM in climate realizations that preclude meeting the CO_2 cap. The EDM includes several constraints from the CEM, including balancing supply and demand within each of our five subregions while accounting for transmission inflows and outflows; constraining regional monthly hydropower generation to an energy budget; constraining wind and solar generation to spatially- and temporally-differentiated capacity factors; and constraining fossil-based thermal plant generation based on capacity deratings. Since we cannot probabilistically sample generator outages like hourly resource adequacy models, the EDM instead derates generators' capacities based on temperature-dependent or fixed forced outage rates (FORs). We run the EDM for a 1-year optimization horizon. Inputs to the EDM include a decarbonization pathway and variables driven by the given climate ensemble member (i.e., daily electricity demand, monthly hydroelectric generation, daily solar and wind capacity factors, and daily thermal plant forced outage rates and derates). See SI.F for the full EDM formulation and key parameters.

From the EDM output, we directly obtain daily ENS and calculate SAC for each region. SAC equals daily available non-hydropower capacity, hydropower generation, and transmission imports minus demand and transmission exports for each region. In this way, SAC indicates excess supply available in a region to satisfy unexpected increases in demand. The lower the SAC, the greater the risk of a supply shortfall, suggesting lower resource adequacy. Prior research has used a net load metric as a proxy for resource adequacy [55, 62]. Our SAC extends the net load metric by capturing not just daily wind and solar generation potential, but also accounts for optimized hydroelectric dispatch; temperature dependent outages in thermal and hydroelectric power plants; capacity deratings in fossil-based thermal power plants; and electricity flows between regions. See SI.G for more details on SAC calculation.

2.4 LENS2 Climate Data and Conversion to Power System Variables

In the near-term (prior to 2050), internal variability (versus model or emissions scenario uncertainty) is the primary source of climate-related uncertainty [37, 39]. To capture the role of internal variability in driving potential climates through 2040, we use the CESM2 Large Ensemble (LENS2) [60]. This dataset is a single model initial-condition large ensemble (SMILE) following the SSP3-7.0 emissions trajectory. We treat this global emissions trajectory as independent of our system's emissions trajectory, as internal variability - not emissions uncertainty - is the primary source of uncertainty over our study period.

The LENS2 dataset consists of 100 ensemble members which are split into 2 groups each consisting of 50 realizations, where each group is driven by one forcing condition. Each of the 50 realizations in the two groups are initiated from different initial conditions sampled to reflect micro and macro perturbations in the pre-industrial control simulation. Unless noted otherwise, all the variables with a specified frequency represent an average over the inherent time periods, e.g. daily temperature is daily averaged temperatures and monthly runoffs are monthly averaged runoffs. We obtain daily surface temperature, 10m wind speed, surface downwelling solar flux, surface atmospheric pressure, surface relative humidity, and monthly surface liquid runoff from 1980-2050 for each ensemble member. We obtain these variables at the highest spatial resolution possible, at a 100 km by 100 km grid. While this spatial and temporal resolution is lower than what is preferred for power system modeling, higher resolution climate datasets (e.g., from statistical or dynamical downscaling) often do not sample as large of a range of internal climate variability as LENS2, particularly in the time-span of interest to us (through 2040) and when focusing on extreme events. On the other hand, this approach does not sample climate response uncertainty, i.e., how different climate models portray the future response to greenhouse gas forcing.. We discuss the value of using a large ensemble like LENS2 and how it can assist creation of higher resolution products in our Discussion. More information on these variables are in SI.B.

We apply a mean bias correction to LENS2 surface temperatures using surface temperatures from the ERA5 reanalysis data [63, 64]. To bias correct runoff for forecasting hydroelectric generation, we use a mean bias scaling method for each of the constituent drought regions [ref B.3]. More details on the bias correction methods are in SI.B.1. Other studies using large ensembles for quantifying climate impacts have also used such mean bias correction methods [39]. We do not use more sophisticated bias correction methods like quantile mapping (QM) as it fits the distribution of projections to observations (historical climate), which may lead to loss of changes in internal variability in the projections. We do not find a strong bias in solar radiation, so we did not bias correct it. Though we identify biases in 10 m wind speeds relative to ERA5, wind power capacity factors derived from bias corrected wind speeds are much lower compared to other observational datasets. As a result, we use the native LENS2 wind speed data in our analysis.

We use different models to derive power system variables from LENS2 data. We calculate daily solar and wind capacity factors for each LENS2 grid cell using deterministic equations (SI.B.2). We calculate monthly hydroelectric generation using a linear regression model using surface runoff as the predictor variable. We obtain the model for each drought region in the Western US [65] by training observed hydroelectric generation [66] trained against ERA5 surface runoff. We then forecast hydroelectric generation using bias corrected surface runoff from the LENS2 data (SI.B.3). We calculate demand for each of our five subregions using a piecewise linear regression model using daily temperature as the predictor variable. The regression model is trained using observed demand data and ERA5 surface temperatures, so ignores technological or population changes (SI.C). We calculate temperature-dependent forced outage rates for thermal power plants using plant-type-specific relationships [67] (SI.D). We also calculate capacity deratings of fossil-based thermal power plants for each LENS2 grid cell using plant-type-specific relationships between deratings and air temperatures, relative humidity, and/or air pressure (SI.D).

3 Results

3.1 Capacity Investments across Decarbonization Pathways

We first examine the five decarbonization pathways output by our capacity expansion model. In creating these pathways using five sampled LENS2 ensemble members rather than creating 100 pathways using each of the 100 LENS2 ensemble members, we demonstrate the value of our framework in analyzing a limited number of alternatives generated by computationally complex planning models, similar to how alternatives are incorporated in system planning in practice. Each pathway is defined by its "fleet" of energy generator types. Our pathways decarbonize primarily through investment in wind and solar capacity, but exhibit different levels of investment (Figure 2). Interconnect-wide solar and wind capacity increase from roughly 40 and 30 GW in 2022, respectively, to up to 129 and 46 GW in 2040, respectively, across pathways. Between pathways, wind and solar capacities in 2040 range from 34 to 46 GW and from 103 to 129 GW, respectively. Small amounts (less than 4 GW) of NGCC with carbon capture and sequestration (CCS) are also deployed in four decarbonization pathways. Heterogeneity in solar and natural gas capacity largely drives differences in total installed capacity between pathways, which ranges from 252 to 280 GW. Solar capacity investment largely occurs in three regions - California, Desert Southwest, and Central - with high quality solar resources, while wind investment largely occurs in the Northwest, which has high quality wind resources (Figure A.1). No investment in interregional transmission beyond existing capacity occurs. Growth in wind, solar, and NGCC capacity displace other capacity, including coal-fired capacity, and replace lost capacity from the retirement of the Diablo Canyon nuclear generating station. Generation by plant type follows similar trends as capacity investments. Across pathways, wind, solar, natural gas, and hydropower account for roughly 7-13%, 31-37%, 23-27%, and 20-24% of annual generation, respectively, in 2040.

3.2 Resource Adequacy of Decarbonization Pathways under Future Climate Realizations

For each decarbonization pathway, we use LENS2 to quantify daily electricity supply and demand under 100 potential climate realizations in any given year. Using daily supply and demand, we approximate resource adequacy through two metrics: daily surplus available capacity (SAC) and daily energy not served (ENS), both quantified in units of electricity. SAC indicates excess electricity supply available in a region to satisfy unexpected increases in demand, while ENS equals the difference between electricity demand and supply. A negative daily SAC value indicates ENS occurs, while larger positive SAC values indicate greater redundancy against supply shortfalls. Given daily SAC and ENS for each of our five decarbonization pathways under each of our 100 ensemble members, we then calculate the annual minimum SAC ("minimum SAC"),

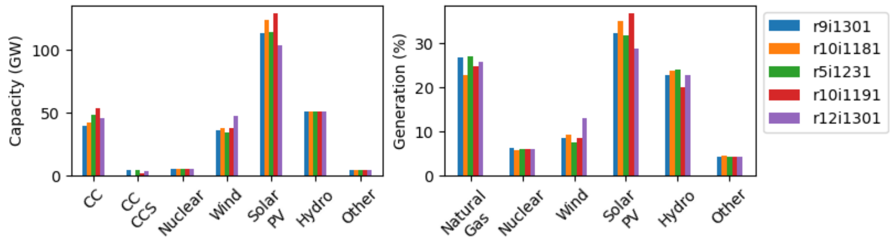

Fig. 2: (a) Installed capacity and (b) electricity generation by generator type across Western Interconnect in 2040 for each decarbonization pathway, which are labeled by the LENS2 ensemble member used to drive the capacity expansion model (detailed in Section 4.2). CC stands for natural gas combined cycle, CCCCS for CC with carbon capture and sequestration, and PV for photovoltaic.

which indicates the fleet's largest susceptibility to supply shortfalls in a given year, and total annual ENS ("total ENS"), which indicates the fleet's total supply shortfall in a given year.

Figures 3 and A.2 show these two metrics for our three largest regions by demand (California, Desert Southwest, and Northwest) and the Western Interconnect in 2040. Depending on the region, resource adequacy failures occur in most or all decarbonization pathways under many climate realizations, as indicated by negative SAC values and positive total ENS values. Pathways exhibit significant differences in resource adequacy under future climate realizations. For instance, in California in 2040, one decarbonization pathway ("r9i1301", or the pathway generated using the r9i1301 climate ensemble member) has a maxiumum of 286 GWh of total yearly ENS, whereas the other pathways have maximum total yearly ENS of 0-100 GWh, respectively. Across decarbonization pathways, certain climate realizations incur significantly greater ENS than others (as indicated by vertical red stripes). For instance, of the total ENS across all 2040 California pathways and all 100 climate realizations, none of that ENS occurs in 79% of climate realizations, while 50% of that ENS occurs in just 3% of climate realizations. Maximum ENS values are largely driven by days with low hydropower and coinciding low wind and solar generation (Figures A.3 - A.7).

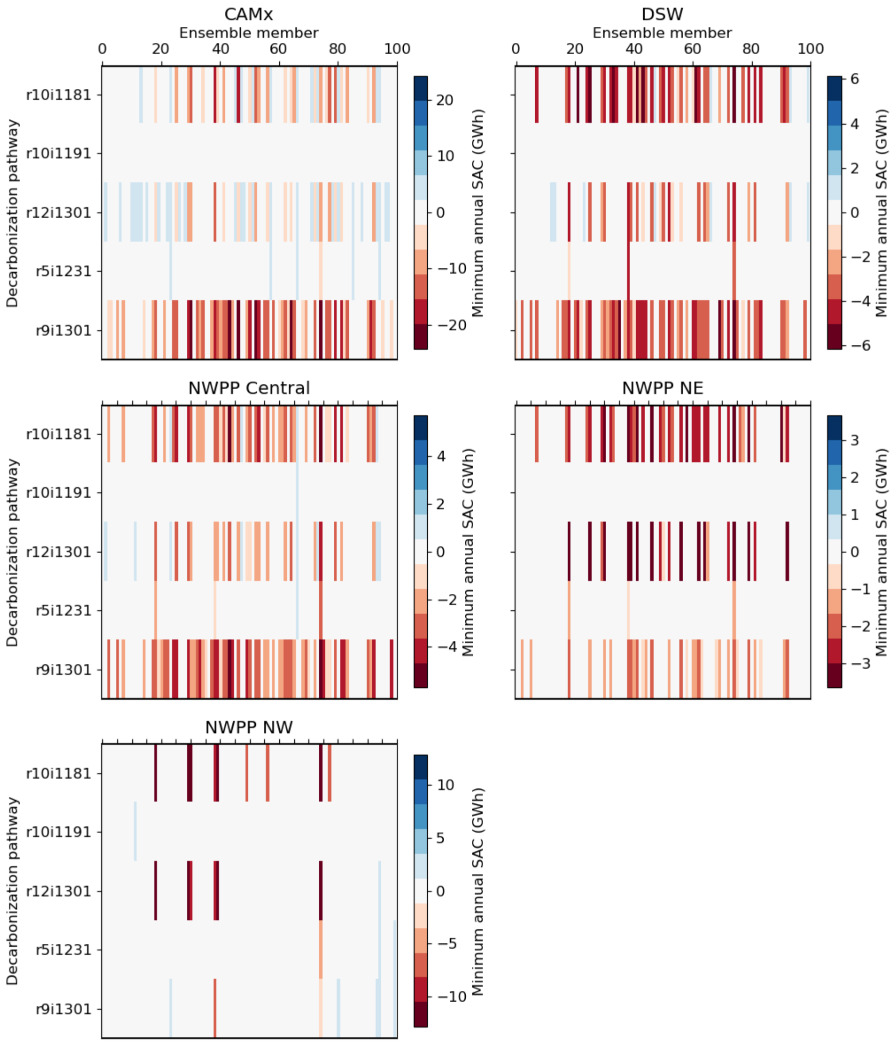

Fig. 3: Minimum annual SAC values for each subregion in 2040 (see Fig. 1 for map of regions). Each panel corresponds to a realization of the lower right panel of Fig. 1. Each row corresponds to one of the five decarbonization pathways, labeled by the sampled ensemble member used in the capacity expansion model to create the pathway. Within each row, there are 100 separate color bars that indicate that pathway's minimum annual SAC against each of our 100 climate ensemble members. Minimum annual SAC values range from negative (red) to positive (blue) red values indicate supply shortfalls (or resource adequacy failures), while blue values indicate surplus capacity relative to demand.

3.3 Carbon Dioxide Emissions and Costs of Decarbonization Pathways under Climate Realizations

Future climate variability will affect not only the resource adequacy of future fleets, but also their CO_2 emissions and operational costs through changes in electricity demand; available wind, solar, and hydropower potential; and generation from dispatchable (largely fossil) plants (Figure 4). Across our decarbonization pathways, climate realizations could result in CO_2 emissions higher or lower than the CO_2 cap by up to 28% and 27%, respectively. As with resource adequacy (Figure 3), CO_2 emissions from some decarbonization pathways are less vulnerable to climate variability than others. For instance, one pathway ("r5i1231", or generated using the r5i1231 climate ensemble member) fails to meet the CO_2 emissions cap in 70% of climate realizations, while another pathway ("r10i1191") only fails to meet the emissions cap in 20% of realizations. Operational costs also vary across climate realizations in each pathway, from $127 to $146 billion. No single meteorological variable drives the observed variability in emissions and costs (Figure A.9). Rather, high emissions generally occur in climate realizations with low wind, solar, and hydropower generation and high demand.

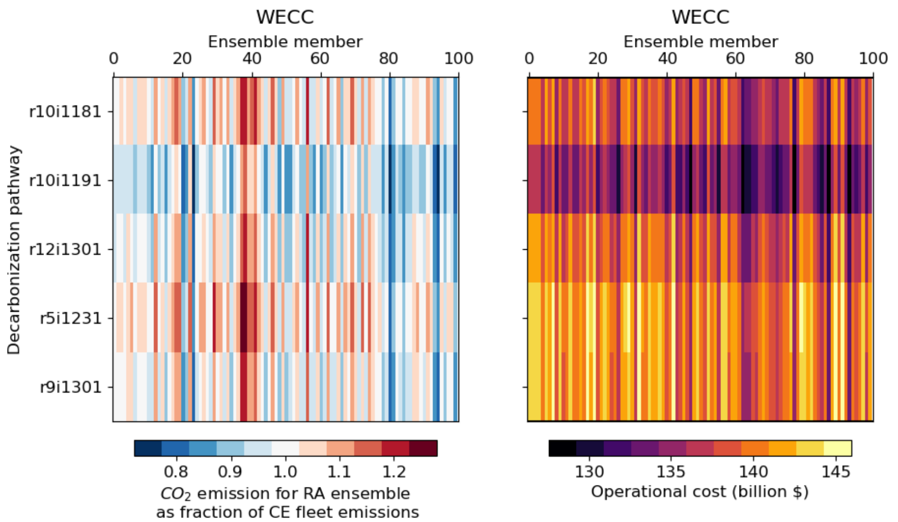

Fig. 4: Same structure as Figure 3, but each color bar shows interconnect-wide CO_2 emissions as a fraction of the target CO_2 emissions cap (left) or interconnect-wide operational costs (right) in 2040.

3.4 Trade-offs between Resource Adequacy and Costs

Power system planners must balance competing objectives of minimizing system costs while meeting resource adequacy targets. Figure 5 compares each decarbonization pathway's total costs against the sum of annual minimum SAC over the five sub-regions (Figure 3) across 2040 climate realizations. Total costs include fixed investment costs, which vary between decarbonization pathways but not climate realizations, and operational costs (Figure 4), which vary between decarbonization pathways and climate realizations. Cumulative total costs from 2023 to 2040 range from $223-246 billion across pathways and climate variability. Although pathways are differentiated by their mean costs across realizations, variability in operational costs induced by climate variability introduces overlap in total cost ranges between pathways. Despite overlaps between total costs, pathways can exhibit significant differences in resource adequacy outcomes. For instance, one pathway ("r10i1191", or the second pathway from the right in Figure 5) only exhibits a small resource adequacy failure (or a total regional minimum annual SAC value of -0.2 GWh) under one climate realization, and has a positive mean SAC value across ensemble members. Other pathways (e.g., the three pathways at left in Figure 5) have larger resource adequacy failures (of up to -40 GWh SAC) under certain ensemble members, and negative mean SAC values across ensemble members (of up to -10 GWh). Selecting the r10i1191 pathway rather than other pathways would eliminate resource adequacy failures at a median total cost difference of -1 to 3%.

3.5 Identifying an Alternative Decarbonization Pathway Robust to Future Climate Realizations

Our prior results indicate a subset of potential climate realizations drive significant risk of resource adequacy failures across decarbonization pathways (Figure 3). We identify the ensemble member that drives the largest resource adequacy failures (quantified as the sum of minimum annual SACs) across decarbonization pathways in California (our largest load region) in 2040, namely r19i1231, then rerun our capacity expansion model using that ensemble member's meteorology. This ensemble member was not captured in our initial sampling procedure, in which we selected five ensemble members that spanned the warming at mid-century represented by the ensembles in the CESM2-LE dataset (Figure B.10). Rather, r19i1231 features a compound extreme event in 2040 of low hydropower and wind generation potential and high air temperatures, the latter of which drive elevated electricity demand and low available thermal capacity (Figure A.10). Capturing unexpected extreme climate realizations, such as r19i1231, is a key motivator for our framework, as identifying extremes a priori is difficult given complex interactions within power systems.

Our new decarbonization pathway generated with the r19i1231 climate ensemble member invests in more solar and NGCC capacity and in less wind capacity than other pathways (Figure 6a). Figure 6b compares the resource

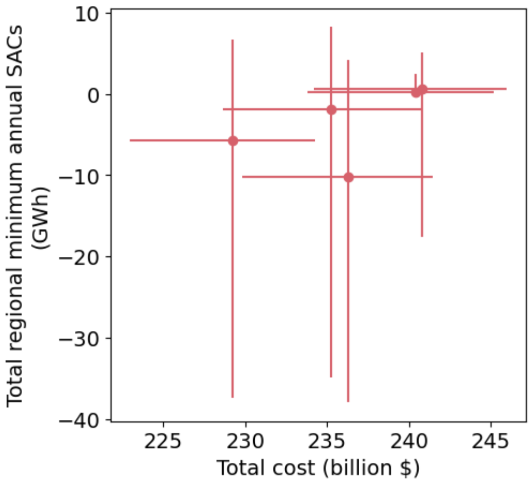

Fig. 5: Interconnect-wide minimum annual SAC Sum of minimum annual SAC values for our five subregions in 2040 versus cumulative (2023-2040) total (fixed plus operating) costs for each decarbonization pathway. Minimum annual SAC values equal the sum of non-synchronous subregional minimum SAC values. Each decarbonization pathway is depicted with a cross; the dot at the center of each cross indicates the mean total SAC and mean total cost for that decarbonization pathway across all 100 climate ensemble members; the horizontal arm of each cross ranges from the minimum to maximum total cost for that decarbonization pathway across all 100 climate ensemble members; and the vertical arm of each cross ranges from the minimum to maximum total SACs for that decarbonization pathway across all 100 climate ensemble members. For context, total non-synchronous peak demand across the five subregions equals roughly 200 GWh (although peak demand varies across climate realizations). A negative minimum annual SAC value indicates one or more subregions in that pathway experiences a supply shortfall under at least one future climate realization.

adequacy of the decarbonization pathway generated with this new ensemble member versus our original decarbonization pathways. Our new pathway exhibits significantly higher minimum SAC values, indicating less vulnerability to resource adequacy failures. In fact, the new pathway does not experience any resource adequacy failures across any climate realizations in 2040 in any region (i.e., no ENS or negative SAC values), and has a minimum annual SAC of 0-3 GWh in California across climate realizations. The newly generated pathway also meets CO_2 emission caps in all but three potential climate realizations (Figure 6c). Figure 6d compares the trade-off between resource adequacy and system costs for the new versus prior pathways. The new pathway has significantly better resource adequacy than prior pathways, but at greater total costs. Specifically, the new pathway incurs, on average, roughly

$10 billion greater total costs between 2023 and 2040 compared to the next costliest pathway.

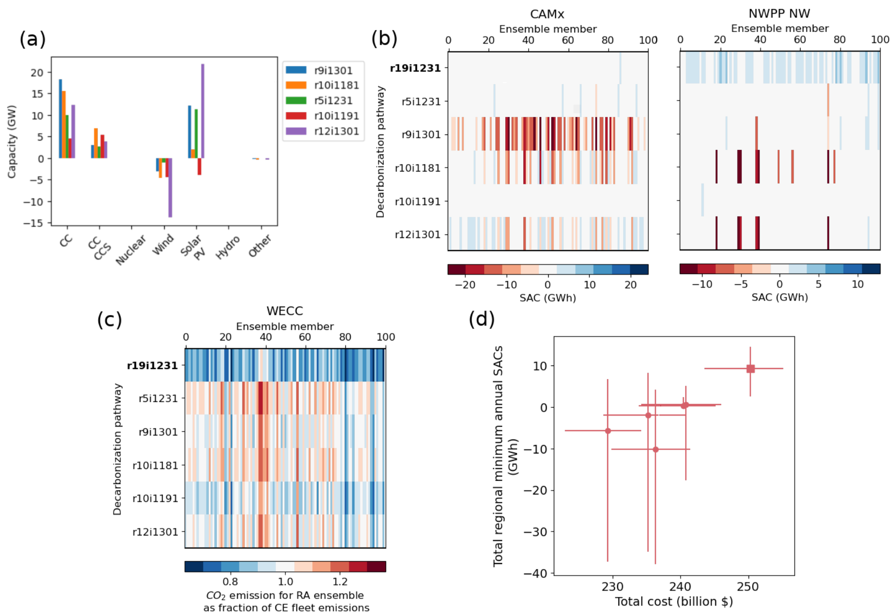

Fig. 6: (a) Difference in installed capacity by generator type across Western Interconnect in 2040 between the decarbonizatoin pathway generated using the r19i1231 ensemble member and each of the other driving ensemble members. CC stands for natural gas combined cycle, CCCCS for CC with carbon capture and sequestration, and PV for photovoltaic. (b) Same structure as Figure 3, but includes the decarbonization pathway generated using the r19i1231 ensemble member (bolded at top) and only includes the two largest subregions by demand for conciseness. (c) Same structure as left panel of Figure 3.3, but includes the decarbonization pathway generated using the r19i1231 ensemble member (bolded at top). (d) Same structure as left panel of Figure 5, but includes the decarbonization pathway generated using the r19i1231 ensemble member (shown as cross centered on square instead of circle).

4 Discussion

Existing research and system planning practices lack decision support frameworks for identifying investment alternatives that are robust to climate-related uncertainty. We construct such an analytical framework by integrating planning and operational power system models with a large climate ensemble, then use our framework to identify the vulnerabilities, trade-offs, and robustness of alternative decarbonization pathways for the Western U.S. power system in 2040. We began our analysis with five alternative pathways to 60% decarbonization of the power system. All of these pathways exhibited modest to significant resource adequacy failures under potential climate realizations. But by choosing one pathway over others, significantly better resource adequacy outcomes can be achieved at little additional cost. Even this more robust pathway, though, suffered resource adequacy losses under future climate realizations. By identifying a particularly problematic future climate realization for future resource adequacy and using it to create another alternative decarbonization pathway, we identified a pathway robust to, or that experienced no resource adequacy failures under, all examined future climate realizations. This robustness is achieved through an increase of roughly $10 billion (or 5%) in total costs, posing a trade-off to decision-makers.

Our analysis quantifies the resource adequacy of alternative decarbonization pathways against an unprecedented range of near-term climate variability. Capturing this range of climate variability was possible through the use of the LENS2 dataset, but came at the cost of climate data with poor spatial and temporal resolution. Energy system modeling needs and available climate dataset characteristics are often misaligned [25], and conducting detailed downscaling of all LENS2 ensemble members is computationally prohibitive. However, our analytical framework can guide high resolution downscaling of large climate ensembles like LENS2 for energy system applications, a key need for energy system modelers. Specifically, our framework can identify ensemble members, periods of interest, and/or climate conditions that pose the greatest threat to alternative future power systems. Threatening conditions are themselves a function of investment decisions in power systems, so identifying those conditions for a broad range of alternatives, as our framework enables, is crucial to fully characterize vulnerabilities and robustness. In our case, one ensemble member (r19i1231) resulted in resource adequacy failures across nearly all studied decarbonization targets due to the compounding effects of low wind and hydropower generation potential and high air temperatures. Identified members, periods, or climate conditions of concern can be selectively downscaled and fed back into planning or resource adequacy modeling, maximizing the value of high resolution downscaled data. This process requires bottom-up trans-disciplinary collaboration between energy system and climate modellers [25]. In using climate data with poor spatial (100 by 100 km) and temporal (daily) resolution, our analysis is unable to capture the diurnal pattern of solar power, which could bias our investment decisions and resource adequacy analyses in favor of solar power.

Additional opportunities for extending our research exist. We do not consider changes in demand due to adoption of new technologies, e.g. heat pumps to electrify space heating or space cooling in response to increasing temperatures. In winter peaking regions like the Northwest, electrified heating through heat pumps can lead to higher demand in the winter months, introducing interactions between decarbonization and climate change that could affect our SAC calculations. In the Northwest and other regions with historically low space cooling penetrations, adoption of space cooling could also interact with increasing extreme heat to exacerbate summer peak demands. Incorporating the effect of such demand-side changes in our models will allow us to make accurate assessment of future fleets' robustness [9]. Future research could also extend our framework to incorporate additional robustness concepts. For instance, in practice utilities design future systems that meet certain resource adequacy thresholds, e.g. the 1-in-10 standard, which could be captured using a satisficing metric.

Our framework provides a practical way for real-world system planners and utilities to better account for climate-related uncertainty, whether planning for individual or multiple regions. Many planners and utilities use third-party software packages, e.g. PLEXOS or RESOLVE, to make long-term plans. Modifying the underlying mathematical formulation used in these packages, e.g., from a deterministic to stochastic or robust optimization, is challenging for end users. Conversely, our framework only requires changes to model inputs and additional processing of model results, a more feasible undertaking. Planners could obtain a range of climate realizations of interest, ideally in collaboration with climate scientists, then stress test their alternative plans against those climate realizations to identify system vulnerabilities and challenging climate realizations. Challenging climate realizations can then be downscaled and used in more detailed analyses, saving time and effort when compared to downscaling all realizations. Planners could further feed generated insights back into their pipeline, as we demonstrated above, to identify potentially more robust investment plans. Regulators could also require utilities to engage in stress testing during Integrated Resource Plan (IRP) proceedings to understand trade-offs between improved resource adequacy and greater consumer costs. Through practical applications like these, our framework can help practitioners identify future power systems that are robust to climate change and that simultaneously advance reliable, affordable, and clean objectives.

5 Acknowledgements

Michael Craig and Srihari Sundar thank the U.S. National Science Foundation under Award Number 2142421 for funding this work. Many visualizations were created with Seaborn [68]. They thank the CESM2 Large Ensemble Community Project and supercomputing resources provided by the IBS Center for Climate Physics in South Korea. Flavio Lehner acknowledges support from the U.S. Department of Energy, Office of Science, Office of Biological & Environmental Research (BER), Regional and Global Model Analysis (RGMA) component of the Earth and Environmental System Modeling Program under Award Number DE-SC0022070 and National Science Foundation (NSF) IA 1947282. The National Center for Atmospheric Research is sponsored by the National Science Foundation. Nathalie Voisin was supported by the GODEEEP Investment at Pacific Northwest National Laboratory (PNNL).

PNNL is a multi-program national laboratory operated for the U.S. Department of Energy (DOE) by Battelle Memorial Institute under Contract No. DE-AC05-76RL01830. The views and opinions of authors expressed herein do not necessarily state or reflect those of the United States Government or any agency thereof.

6 Data availability

Meteorological data used in this study is available through [60]. Code for the CEM, SAC calculations, and analysis notebook used to create figures in the manuscript are available at https://github.com/ASSET-Lab/WesternUSRDM. Processed meteorological fields and data used in the analysis will be archived in Zenodo. Analysis data is available temporarily at WesternUSRDM-drive.

References

[1] Clarke, L., Wei, Y.-M., Navarro, A.D.L.V., Garg, A., Hahmann, A.N., Khennas, S., Azevedo, I.M.L., Löschel, A., Singh, A.K., Steg, L., Strbac, G., Wada, K.: Energy Systems. In: Shukla, P.R., Skea, J., Slade, R., Khourdajie, A.A., van Diemen, R., McCollum, D., Pathak, M., Some, S., Vyas, P., Fradera, R., Belkacemi, M., Hasija, A., Lisboa, G., Luz, S., Malley, J. (eds.) IPCC, 2022: Climate Change 2022: Mitigation of Climate Change. Contribution of Working Group III to the Sixth Assessment Report of the Intergovernmental Panel on Climate Change. Cambridge University Press, Cambridge, UK and New York, NY, USA (2022). Chap. 6. https://doi.org/10.1017/9781009157926.008

[2] Rogelj, J., Schaeffer, M., Meinshausen, M., Knutti, R., Alcamo, J., Riahi, K., Hare, W.: Zero emission targets as long-term global goals for climate protection. Environmental Research Letters **10**(10), 105007 (2015)

[3] National Academies of Sciences, Engineering, and Medicine, et al.: Accelerating decarbonization of the us energy system (2021)

[4] Jenkins, J.D., Mayfield, E.N., Farbes, J., Jones, R., Patankar, N., Xu, Q., Schivley, G.: Preliminary report: The climate and energy impacts of the inflation reduction act of 2022. REPEAT Project, Princeton, NJ (2022)

[5] Ralston Fonseca, F., Craig, M., Jaramillo, P., Bergés, M., Severnini, E., Loew, A., Zhai, H., Cheng, Y., Nijssen, B., Voisin, N., Yearsley, J.: Effects of Climate Change on Capacity Expansion Decisions of an Electricity Generation Fleet in the Southeast U.S. Environ. Sci. Technol. (2021). https://doi.org/10.1021/acs.est.0c06547

[6] Denholm, P., Brown, P., Cole, W., Mai, T., Sergi, B., Brown, M., Jadun,

P., Ho, J., Mayernik, J., McMillan, C., Sreenath, R.: Examining supply-side options to achieve 100% clean electricity by 2035 (2022)

[7] Cole, W., Carag, J.V., Brown, M., Brown, P., Cohen, S., Eurek, K., Frazier, W., Gagnon, P., Grue, N., Ho, J., Lopez, A., Mai, T., Mowers, M., Murphy, C., Sergi, B., Steinberg, D., Williams, T.: 2021 standard scenarios report: A u.s. electricity sector outlook. NREL (2021). https://doi.org/10.2172/1834042

[8] Jenkins, J.D., Mayfield, E.N., Larson, E.D., Pacala, S.W., Greig, C.: Mission net-zero america: The nation-building path to a prosperous, net-zero emissions economy. Joule **5**(11), 2755–2761 (2021)

[9] Wessel, J., Kern, J.D., Voisin, N., Oikonomou, K., Haas, J.: Technology pathways could help drive the us west coast grid's exposure to hydrometeorological uncertainty. Earth's Future **10**(1), 2021–002187 (2022)

[10] Davis, S.J., Lewis, N.S., Shaner, M., Aggarwal, S., Arent, D., Azevedo, I.L., Benson, S.M., Bradley, T., Brouwer, J., Chiang, Y.-M., *et al.*: Net-zero emissions energy systems. Science **360**(6396), 9793 (2018)

[11] Berrill, P., Wilson, E.J., Reyna, J.L., Fontanini, A.D., Hertwich, E.G.: Decarbonization pathways for the residential sector in the united states. Nature Climate Change **12**(8), 712–718 (2022)

[12] Lee, H., Calvin, K., Dasgupta, D., Krinner, G., Mukherji, A., Thorne, P.: Synthesis report of the ipcc sixth assessment report (ar6). Intergovernmental Panel on Climate Change, Geneva, Switzerland [Google Scholar] (2023)

[13] Craig, M.T., Cohen, S., Macknick, J., Draxl, C., Guerra, O.J., Sengupta, M., Haupt, S.E., Hodge, B.-M., Brancucci, C.: A review of the potential impacts of climate change on bulk power system planning and operations in the united states. Renewable and Sustainable Energy Reviews **98**, 255–267 (2018)

[14] Auffhammer, M., Baylis, P., Hausman, C.H.: Climate change is projected to have severe impacts on the frequency and intensity of peak electricity demand across the united states. Proceedings of the National Academy of Sciences **114**(8), 1886–1891 (2017)

[15] Ralston Fonseca, F., Jaramillo, P., Bergés, M., Severnini, E.: Seasonal effects of climate change on intra-day electricity demand patterns. Climatic Change **154**, 435–451 (2019)

[16] Miara, A., Macknick, J.E., Vörösmarty, C.J., Tidwell, V.C., Newmark, R.,

Fekete, B.: Climate and water resource change impacts and adaptation potential for us power supply. Nature Climate Change **7**(11), 793–798 (2017)

[17] Henry, C.L., Pratson, L.F.: Effects of environmental temperature change on the efficiency of coal-and natural gas-fired power plants. Environmental science & technology **50**(17), 9764–9772 (2016)

[18] Bartos, M.D., Chester, M.V.: Impacts of climate change on electric power supply in the western united states. Nature Climate Change **5**(8), 748–752 (2015)

[19] Karnauskas, K.B., Lundquist, J.K., Zhang, L.: Southward shift of the global wind energy resource under high carbon dioxide emissions. Nature Geoscience **11**(1), 38–43 (2018)

[20] Turner, S.W., Ng, J.Y., Galelli, S.: Examining global electricity supply vulnerability to climate change using a high-fidelity hydropower dam model. Science of the Total Environment **590**, 663–675 (2017)

[21] Schewe, J., Heinke, J., Gerten, D., Haddeland, I., Arnell, N.W., Clark, D.B., Dankers, R., Eisner, S., Fekete, B.M., Colón-González, F.J., *et al.*: Multimodel assessment of water scarcity under climate change. Proceedings of the National Academy of Sciences **111**(9), 3245–3250 (2014)

[22] Turner, S.W.D., Voisin, N., Fazio, J., Hua, D., Jourabchi, M.: Compound climate events transform electrical power shortfall risk in the Pacific Northwest. Nat. Commun. **10**(1) (2019). https://doi.org/10.1038/s41467-018-07894-4

[23] Ralston Fonseca, F., Craig, M., Jaramillo, P., Bergés, M., Severnini, E., Loew, A., Zhai, H., Cheng, Y., Nijssen, B., Voisin, N., *et al.*: Climate-induced tradeoffs in planning and operating costs of a regional electricity system. Environmental Science & Technology **55**(16), 11204–11215 (2021)

[24] Sundar, S., Craig, M.T., Payne, A.E., Brayshaw, D.J., Lehner, F.: Meteorological drivers of resource adequacy failures in current and high renewable western us power systems. Nature Communications **14**(1), 6379 (2023)

[25] Craig, M.T., Wohland, J., Stoop, L.P., Kies, A., Pickering, B., Bloomfield, H.C., Browell, J., De Felice, M., Dent, C.J., Deroubaix, A., *et al.*: Overcoming the disconnect between energy system and climate modeling. Joule **6**(7), 1405–1417 (2022)

[26] Bloomfield, H., Brayshaw, D., Troccoli, A., Goodess, C., De Felice, M., Dubus, L., Bett, P., Saint-Drenan, Y.-M.: Quantifying the sensitivity of european power systems to energy scenarios and climate change projections. Renewable Energy **164**, 1062–1075 (2021)

[27] Abdin, I., Fang, Y.-P., Zio, E.: A modeling and optimization framework for power systems design with operational flexibility and resilience against extreme heat waves and drought events. Renewable and Sustainable Energy Reviews **112**, 706–719 (2019)

[28] Simoes, S.G., Amorim, F., Siggini, G., Sessa, V., Saint-Drenan, Y.-M., Carvalho, S., Mraihi, H., Assoumou, E.: Climate proofing the renewable electricity deployment in europe-introducing climate variability in large energy systems models. Energy Strategy Reviews **35**, 100657 (2021)

[29] Santos da Silva, S.R., Hejazi, M.I., Iyer, G., Wild, T.B., Binsted, M., Miralles-Wilhelm, F., Patel, P., Snyder, A.C., Vernon, C.R.: Power sector investment implications of climate impacts on renewable resources in latin america and the caribbean. Nature communications **12**(1), 1276 (2021)

[30] Kozarcanin, S., Liu, H., Andresen, G.B.: 21st century climate change impacts on key properties of a large-scale renewable-based electricity system. Joule **3**(4), 992–1005 (2019)

[31] Schlott, M., Kies, A., Brown, T., Schramm, S., Greiner, M.: The impact of climate change on a cost-optimal highly renewable european electricity network. Applied energy **230**, 1645–1659 (2018)

[32] Webster, M., Fisher-Vanden, K., Kumar, V., Lammers, R.B., Perla, J.: Integrated hydrological, power system and economic modelling of climate impacts on electricity demand and cost. Nature Energy **7**(2), 163–169 (2022)

[33] Weaver, C.P., Lempert, R.J., Brown, C., Hall, J.A., Revell, D., Sarewitz, D.: Improving the contribution of climate model information to decision making: the value and demands of robust decision frameworks. Wiley Interdisciplinary Reviews: Climate Change **4**(1), 39–60 (2013)

[34] Marchau, V.A., Walker, W.E., Bloemen, P.J., Popper, S.W.: Decision Making Under Deep Uncertainty: from Theory to Practice. Springer, ??? (2019)

[35] Hawkins, E., Sutton, R.: The potential to narrow uncertainty in regional climate predictions. Bulletin of the American Meteorological Society **90**(8), 1095–1108 (2009)

[36] Deser, C., Phillips, A., Bourdette, V., Teng, H.: Uncertainty in climate

change projections: the role of internal variability. Climate dynamics **38**, 527–546 (2012)

[37] Lehner, F., Deser, C., Maher, N., Marotzke, J., Fischer, E.M., Brunner, L., Knutti, R., Hawkins, E.: Partitioning climate projection uncertainty with multiple large ensembles and cmip5/6. Earth System Dynamics **11**(2), 491–508 (2020)

[38] Lehner, F., Deser, C.: Origin, importance, and predictive limits of internal climate variability. Environmental Research: Climate **2**(2), 023001 (2023)

[39] Schwarzwald, K., Lenssen, N.: The importance of internal climate variability in climate impact projections. Proceedings of the National Academy of Sciences **119**(42), 2208095119 (2022)

[40] Lee, J.-Y., Marotzke, J., Bala, G., Cao, L., Corti, S., Dunne, J.P., Engelbrecht, F., Fischer, E., Fyfe, J.C., Jones, C., et al.: Future global climate: scenario-based projections and near-term information. IPCC (2021)

[41] Brockway, A.M., Wang, L., Dunn, L.N., Callaway, D., Jones, A.: Climate-aware decision-making: lessons for electric grid infrastructure planning and operations. Environmental Research Letters **17**(7), 073002 (2022)

[42] CPUC, CAISO, CEC: Root Cause Analysis: Mid-August 2020 Extreme Heat Wave (2021). http://www.caiso.com/Documents/Final-Root-Cause-Analysis-Mid-August-2020-Extreme-Heat-Wave.pdf

[43] Mays, J., Craig, M.T., Kiesling, L., Macey, J.C., Shaffer, B., Shu, H.: Private risk and social resilience in liberalized electricity markets. Joule (2022)

[44] North American Electric Reliability Corporation: 2021 Long-Term Reliability Assessment (2021). https://www.nerc.com/pa/RAPA/ra/Pages/default.aspx

[45] Lempert, R.J., Groves, D.G.: Identifying and evaluating robust adaptive policy responses to climate change for water management agencies in the american west. Technological Forecasting and Social Change **77**(6), 960–974 (2010)

[46] Giuliani, M., Castelletti, A.: Is robustness really robust? how different definitions of robustness impact decision-making under climate change. Climatic Change **135**(3), 409–424 (2016)

[47] Fischbach, J.R., Siler-Evans, K., Tierney, D., Wilson, M.T., Cook, L.M., May, L.W.: Robust stormwater management in the pittsburgh region. RAND Corporation (2017)

[48] Reis, J., Shortridge, J.E.: Impact of uncertainty parameter distribution on robust decision making outcomes for climate change adaptation under deep uncertainty. Risk Analysis **40**(3), 494–511 (2020)

[49] Shortridge, J.E., Guikema, S.D.: Scenario discovery with multiple criteria: An evaluation of the robust decision-making framework for climate change adaptation. Risk Analysis **36**(12), 2298–2312 (2016)

[50] Markolf, S.A., Hoehne, C., Fraser, A.M., Chester, M.V., Underwood, B.S.: Transportation resilience to climate change and extreme weather events–beyond risk and robustness. Transport Policy **74**, 174–186 (2019)

[51] Smith, R., Zagona, E., Kasprzyk, J., Bonham, N., Alexander, E., Butler, A., Prairie, J., Jerla, C.: Decision science can help address the challenges of long-term planning in the colorado river basin. JAWRA Journal of the American Water Resources Association **58**(5), 735–745 (2022)

[52] Nahmmacher, P., Schmid, E., Pahle, M., Knopf, B.: Strategies against shocks in power systems–an analysis for the case of europe. Energy Economics **59**, 455–465 (2016)

[53] Deser, C., Lehner, F., Rodgers, K.B., Ault, T., Delworth, T.L., DiNezio, P.N., Fiore, A., Frankignoul, C., Fyfe, J.C., Horton, D.E., *et al.*: Insights from earth system model initial-condition large ensembles and future prospects. Nature Climate Change **10**(4), 277–286 (2020)

[54] Maher, N., Milinski, S., Ludwig, R.: Large ensemble climate model simulations: introduction, overview, and future prospects for utilising multiple types of large ensemble. Earth System Dynamics **12**(2), 401–418 (2021)

[55] van der Wiel, K., Stoop, L.P., Van Zuijlen, B., Blackport, R., Van den Broek, M., Selten, F.: Meteorological conditions leading to extreme low variable renewable energy production and extreme high energy shortfall. Renewable and Sustainable Energy Reviews **111**, 261–275 (2019)

[56] van der Wiel, K., Bloomfield, H.C., Lee, R.W., Stoop, L.P., Blackport, R., Screen, J.A., Selten, F.M.: The influence of weather regimes on european renewable energy production and demand. Environmental Research Letters **14**(9), 094010 (2019)

[57] Bevacqua, E., Zappa, G., Lehner, F., Zscheischler, J.: Precipitation trends determine future occurrences of compound hot–dry events. Nature Climate Change **12**(4), 350–355 (2022)

[58] Bevacqua, E., Suarez-Gutierrez, L., Jézéquel, A., Lehner, F., Vrac, M., Yiou, P., Zscheischler, J.: Advancing research on compound weather and

climate events via large ensemble model simulations. Nature Communications **14**(1), 2145 (2023)

[59] WECC: Western Assessment of Resource Adequacy (2022). https://www.wecc.org/Reliability/2022%20Western%20Assessment%20of%20Resource%20Adequacy.pdf

[60] Rodgers, K.B., Lee, S.-S., Rosenbloom, N., Timmermann, A., Danabasoglu, G., Deser, C., Edwards, J., Kim, J.-E., Simpson, I.R., Stein, K., *et al.*: Ubiquity of human-induced changes in climate variability. Earth System Dynamics **12**(4), 1393–1411 (2021)

[61] Jones, A.D., Rastogi, D., Vahmani, P., Stansfield, A., Reed, K., Ullrich, P., Rice, J.S.: Im3/hyperfacets thermodynamic global warming (tgw) simulation datasets. Technical report, MultiSector Dynamics-Living, Intuitive, Value-adding, Environment (2022)

[62] Ruggles, T.H., Caldeira, K.: Wind and solar generation may reduce the inter-annual variability of peak residual load in certain electricity systems. Applied Energy **305**, 117773 (2022)

[63] Maraun, D.: Bias correcting climate change simulations - a critical review. Current Climate Change Reports **2**, 211–220 (2016)

[64] Hersbach, H., Bell, B., Berrisford, P., Biavati, G., Horányi, A., Muñoz Sabater, J., Nicolas, J., Peubey, C., Radu, R., Rozum, I., et al.: Era5 hourly data on single levels from 1979 to present. Copernicus Climate Change Service (C3S) Climate Data Store (CDS) **10** (2018)

[65] Turner, S.W., Voisin, N., Nelson, K.D., Tidwell, V.C.: Drought impacts on hydroelectric power generation in the western united states. Technical report, Pacific Northwest National Lab.(PNNL), Richland, WA (United States) (2022)

[66] Turner, S.W., Voisin, N., Nelson, K.: Revised monthly energy generation estimates for 1,500 hydroelectric power plants in the united states. Scientific Data **9**(1), 675 (2022)

[67] Murphy, S., Sowell, F., Apt, J.: A time-dependent model of generator failures and recoveries captures correlated events and quantifies temperature dependence. Applied Energy **253**, 113513 (2019)

[68] Waskom, M.L.: seaborn: statistical data visualization. Journal of Open Source Software **6**(60), 3021 (2021). https://doi.org/10.21105/joss.03021

[69] Jerez, S., Tobin, I., Vautard, R., Montávez, J.P., López-Romero, J.M., Thais, F., Bartok, B., Christensen, O.B., Colette, A., Déqué, M., Nikulin,

G., Kotlarski, S., Van Meijgaard, E., Teichmann, C., Wild, M.: The impact of climate change on photovoltaic power generation in Europe. Nat. Commun. **6** (2015). https://doi.org/10.1038/ncomms10014

[70] Blair, N., Diorio, N., Freeman, J., Gilman, P., Janzou, S., Neises, T., Wagner, M.: System advisor model (sam) general description (version 2017.9. 5). National Renewable Energy Laboratory Technical Report (2018)

[71] TamizhMani, G., Ji, L., Tang, Y., Petacci, L., Osterwald, C.: Photovoltaic module thermal/wind performance: long-term monitoring and model development for energy rating. In: NCPV and Solar Program Review Meeting Proceedings, 24-26 March 2003, Denver, Colorado (CD-ROM) (2003). National Renewable Energy Lab., Golden, CO.(US)

[72] Ruggles, T.H., Farnham, D.J., Tong, D., Caldeira, K.: Developing reliable hourly electricity demand data through screening and imputation. Scientific data **7**(1), 1–14 (2020)

[73] Akar, S., Beiter, P., Cole, W., Feldman, D., Kurup, P., Lantz, E., Margolis, R., Oladosu, D., Stehly, T., Rhodes, G., et al.: 2020 annual technology baseline (atb) cost and performance data for electricity generation technologies. Technical report, National Renewable Energy Laboratory-Data (NREL-DATA), Golden, CO (United … (2020)

[74] Wu, G.C., Jones, R.A., Leslie, E., Williams, J.H., Pascale, A., Brand, E., Parker, S.S., Cohen, B.S., Fargione, J.E., Souder, J., *et al.*: Minimizing habitat conflicts in meeting net-zero energy targets in the western united states. Proceedings of the National Academy of Sciences **120**(4), 2204098120 (2023)

[75] Miller, L.M., Keith, D.W.: Observation-based solar and wind power capacity factors and power densities. Environmental Research Letters **13**(10), 104008 (2018)

[76] NREL: ReEDS OpenAccess. github (2020). https://github.com/atpham88/ReEDS_OpenAccess

[77] Jenkins, J.D., Sepulveda, N.A.: Enhanced decision support for a changing electricity landscape: the genx configurable electricity resource capacity expansion model (2017)

Supplementary Information for Identifying Robust Energy Decarbonization Pathways in the Presence of Deep Climate Uncertainty

A Results

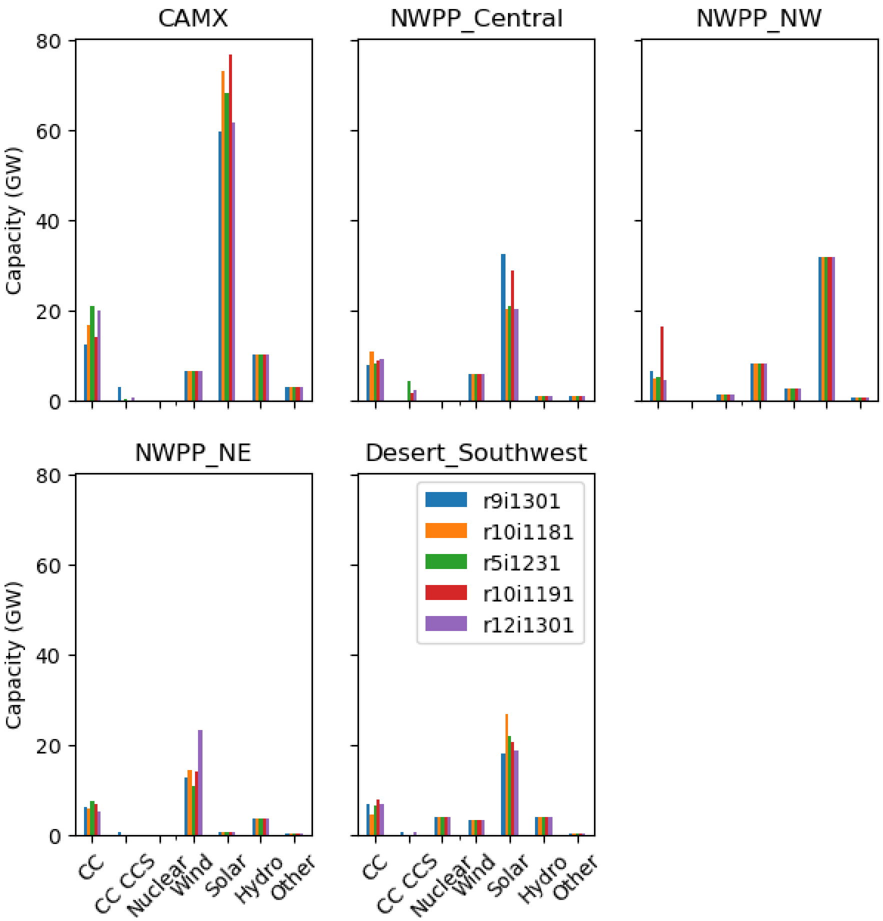

Fig. A.1: Installed capacity of each generator type across each subregion in WECC in the initial fleet (2022) and in 2040. The range bars extend from the mininum to maximum capacity investment across our five initial decarbonization pathways. CC = natural gas combined cycle; HD = hydropower; and NU = nuclear.

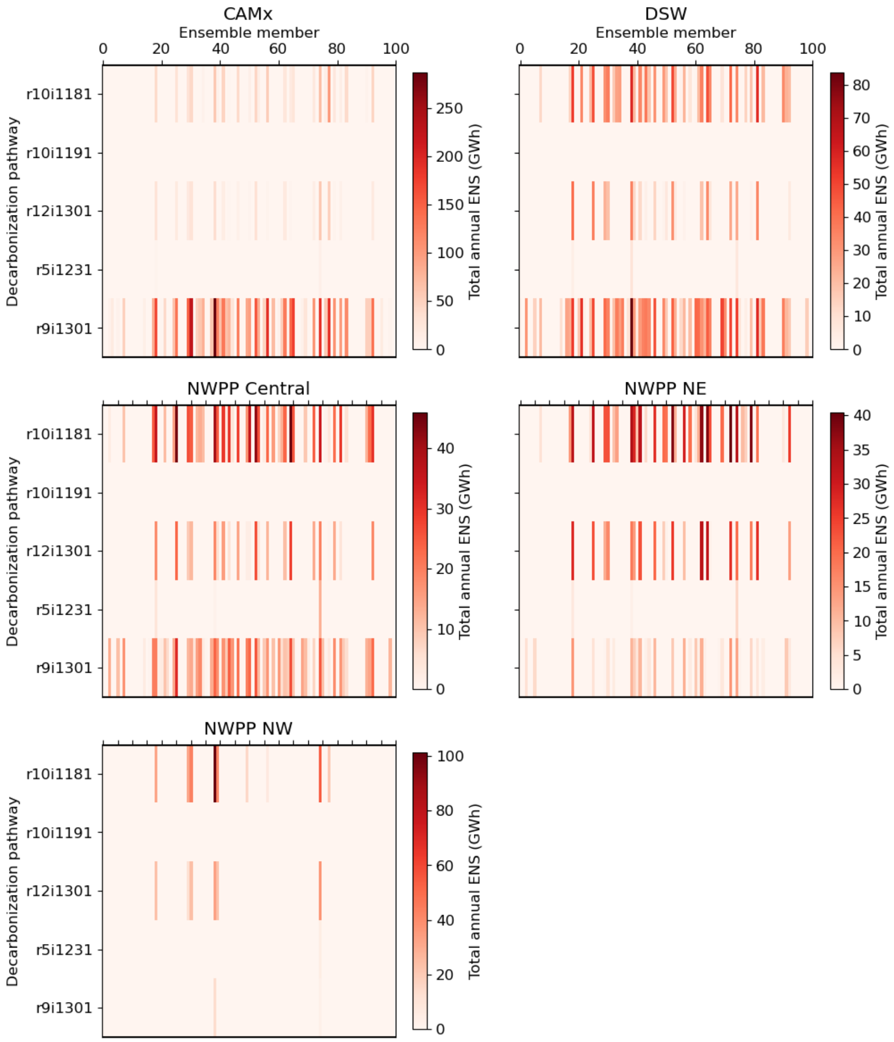

Fig. A.2: Same structure as Figure 3, but each color bar shows total annual energy not served (ENS) rather than minimum annual SAC.

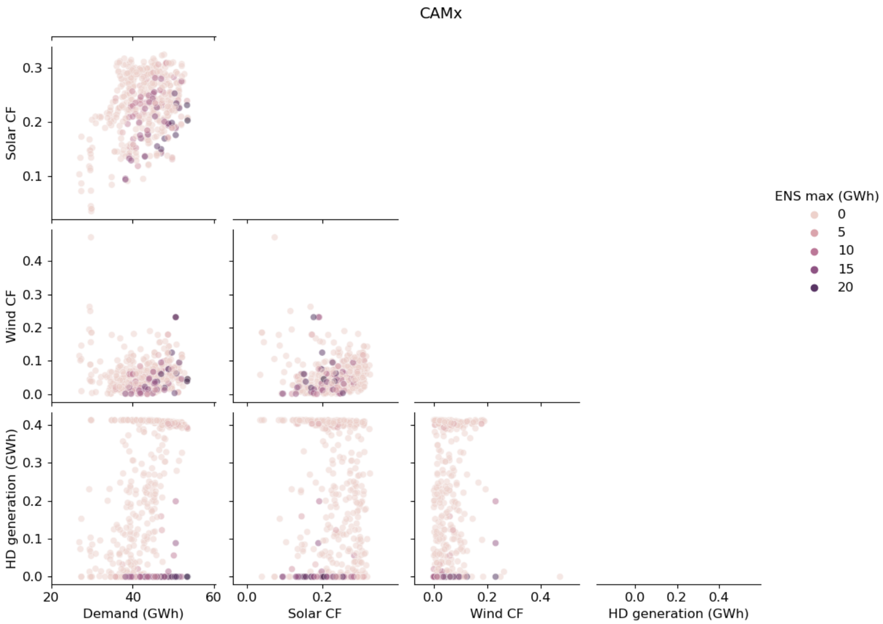

Fig. A.3: Pair plots of weather-driven energy system variables, namely daily electricity demand, solar and wind capacity factors (CF), and hydropower (HD) generation, in California (or our CAMx subregion) in 2040 on the day with the highest annual energy not served. Each plot contains 500 points, which correspond to each of our five initial decarbonization pathways run against each of our 100 ensemble members. Colors indicate ENS magnitude.

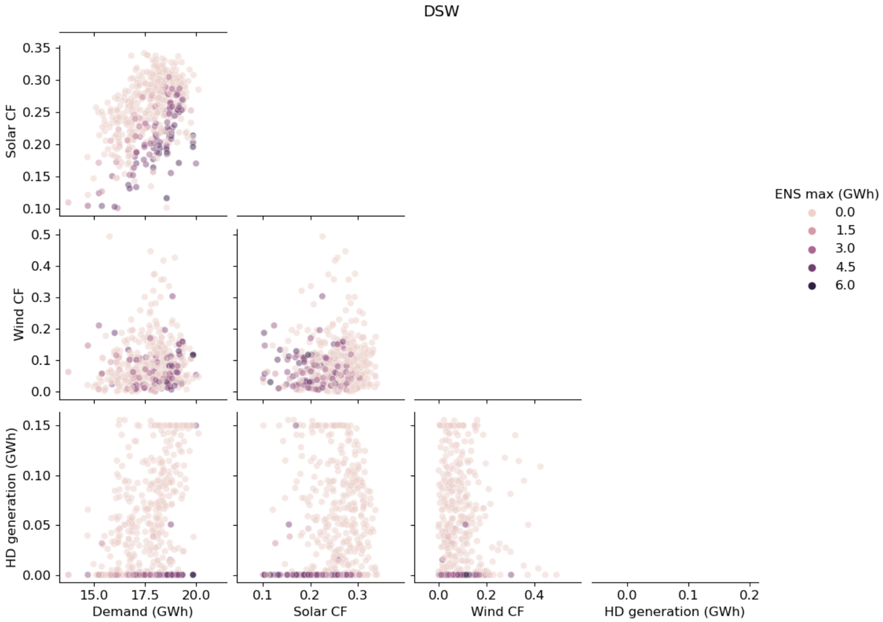

Fig. A.4: Same as figure A.3 but for the Desert Southwest.

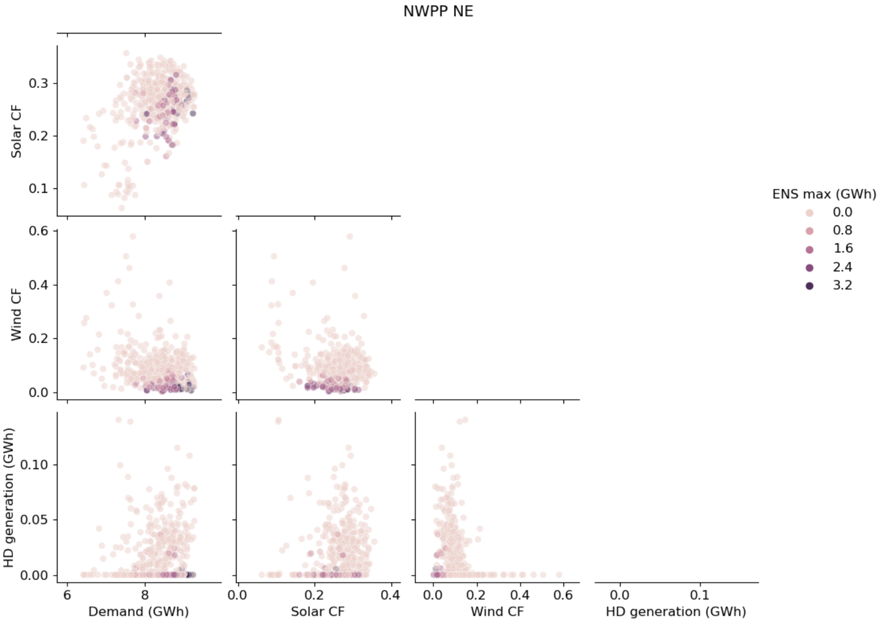

Fig. A.5: Same as figure A.3 but for NWPP NE subregion.

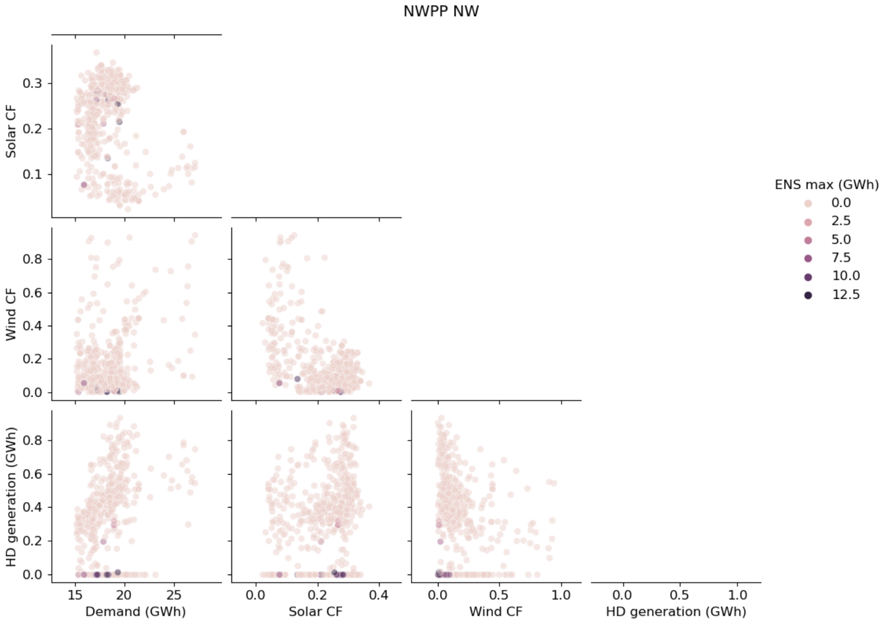

Fig. A.6: Same as figure A.3 but for NWPP NW subregion.

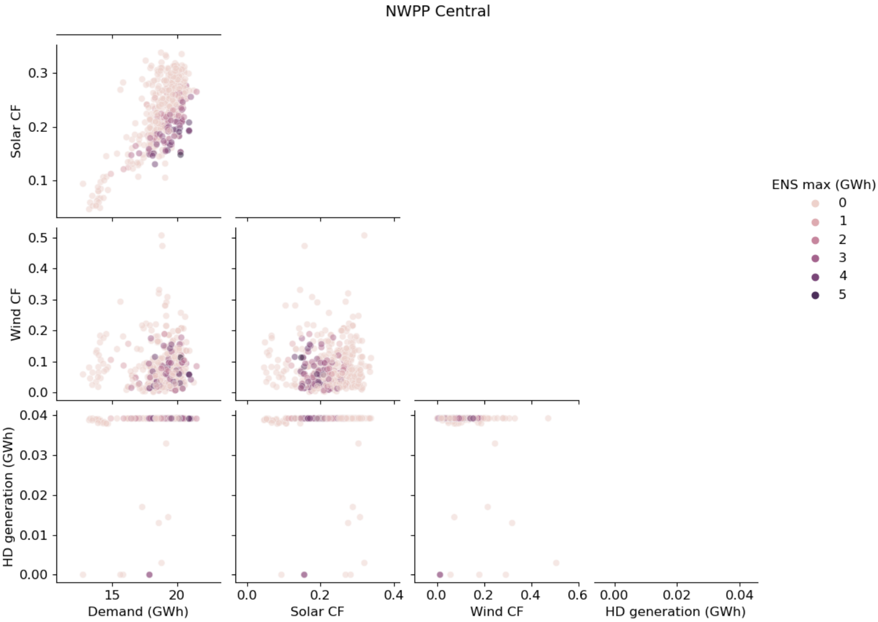

Fig. A.7: Same as figure A.3 but for NWPP Central subregion.

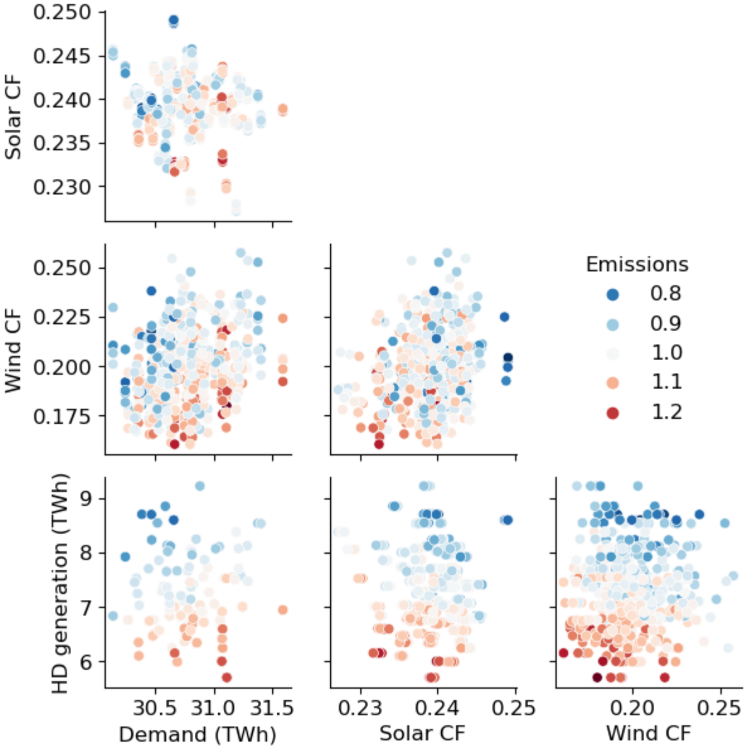

Fig. A.8: For our five initial decarbonization pathways evaluated against all ensemble members for the whole WECC region, this shows pair plots of weather-driven energy system variables: annual average solar capacity factors (CFs), annual average wind CFs, total annual demand, and total annual hydroelectric generation. Points are colored by annual CO_2 emission fractions normalized against the 40% emissions target. Emissions tend to exceed the intended cap in ensemble members with low hydropower generation and coinciding low wind and solar resources.

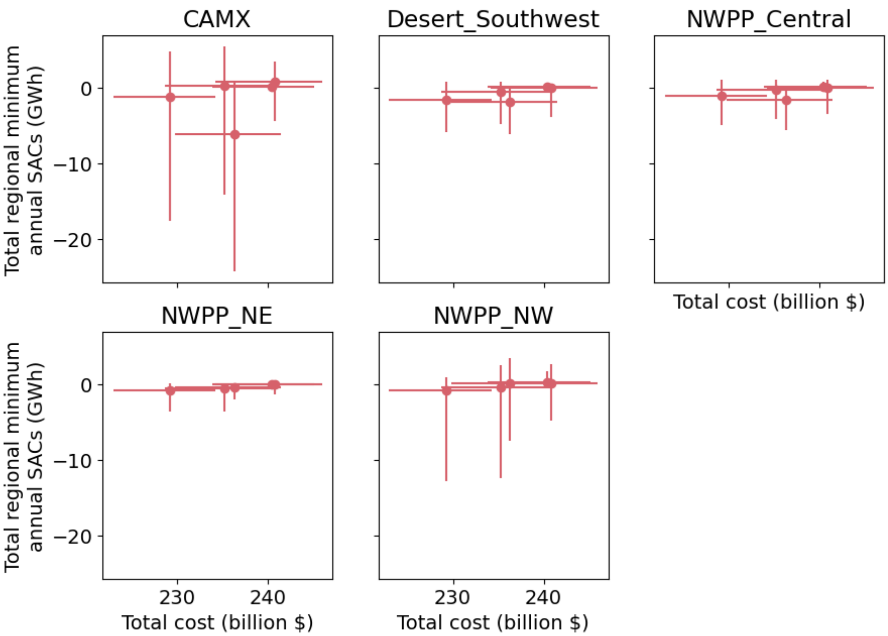

Fig. A.9: Same as figure 5 but the y-axis represents resource adequacy outcomes for each individual region.

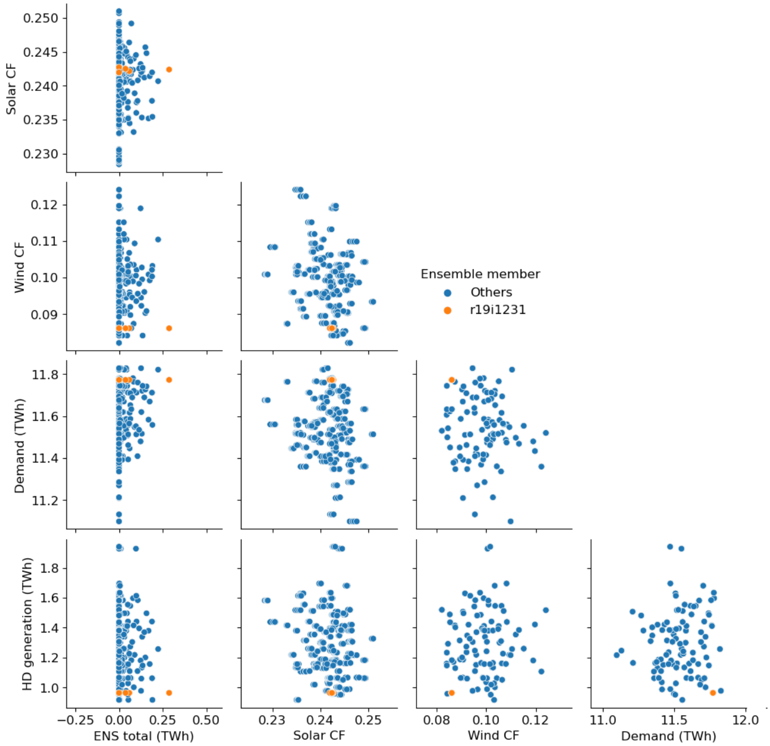

Fig. A.10: Pair plots of weather-driven energy system variables in the five initial decarbonization pathways. Variables are annual average solar and wind capacity factors, total annual daily demand, total annual daily hydroelectric generation, and total annual energy not served. Data is shown for California only, the largest demand region. Yellow dots show outcomes when each pathway is run under the r19i1231p1f2 ensemble member, while blue dots show outcomes while each pathway is run under each of the other 99 ensemble members, thereby illustrating differences between r19i1231p1f2 and other members (high demand, low hydropower, and low wind).

B Climate Data

Variables obtained from CESM2-LE and their features are shown in table 1

Variable Long Name	Short Name	Units	Frequency	Bias Correction Method	Usage in This Study
Reference height temperature	TREFHT	K	Daily	Mean bias shifting	Demand forecasting, power plant derating and outages, solar and wind capacity factors
Downwelling solar flux at surface	FSDS	W/m^2	Daily	-	Solar capacity factors
10m wind speed	U10	m/s	Daily	Mean bias shifting	Solar and wind capacity factors
Surface pressure	PS	Pa	Daily	-	Wind capacity factors, power plant derating
Reference height humidity	QREFHT	kg/kg	Daily	-	Wind capacity factors, power plant derating
Total liquid runoff not including correction for land use change	QRUNOFF	mm/s	Month	Mean bias scaling	Hydroelectric generation

Table 1: Information about CESM2-LE variables obtained, processing applied to them, and their usage.

B.1 Bias Correction

B.1.1 Surface Temperature

1. Get ensemble mean temperature mean over geography of interest
2. Compare with mean of ERA5 temperature regridded to the LENS2 grid over same geography
3. Calculate bias correction factor as $\delta_T = \overline{y_f} - \overline{y_{ra}}$
4. Calculate bias corrected temperature as $y_{f,corr} = y_f - \delta_T$

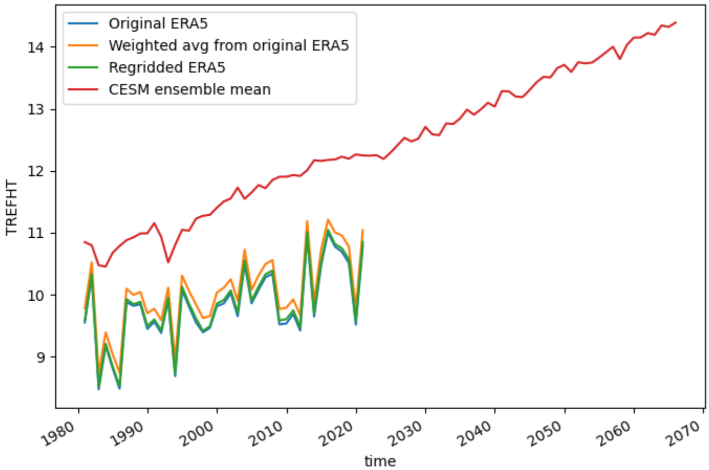

Fig. B.1: Comparison of LENS2 ensemble mean temperature and ERA5 temperature for different methods of averaging.

B.2 Capacity factors

We derive solar capacity factors from surface downwelling shortwave flux data for a EFG-Polycrystalline silicon photovoltaic module using the formulation described by Jerez et. al. [69] [See SI section 1.1]. We calculate wind capacity factors from the 10m wind speed date using the formulation described by Karnauskas et. al. [19] and the composite 1.5 MW IEC class III turbine from the System Advisor Model [70].

B.2.1 Solar

We derive daily solar capacity factors for a EFG-Polycrystalline silicon photovoltaic module as[**?**]:

$$CF_{pv}^{t} = P_{R}^{t} \frac{FSDS^{d}}{RSDS_{STC}} \tag{1}$$

where $RSDS^t$ represents surface downwelling shortwave flux in air $[Wm^{-2}]$ where the superscript d indexes the day. All the metorological variables are discreet in time and space (at the dataset resolution), and the index d is dropped hereafter for conciseness. In eq.1, $RSDS_{STC}$ refers to FSDS at standard test conditions and is equal to $1000Wm^{-2}$, and P_R^t is the performance ratio calculated using

$$P_R = 1 + \gamma[T_{cell} - T_{STC}] \tag{2}$$

$$T_{cell} = c_1 + c_2 TREFHT + c_3 FSDS + c_4 SWS \tag{3}$$

where T_{cell} is the PV cell temperature, TAS is surface air temperature (*2m temperature* and SWS is surface wind speed. In eq.2, $\gamma = -0.005°C^{-1}$ and $T_{STC} = 25°C$. In eq.3, $c_1 = 4.3°C$, $c_2 = 0.943$, $c_3 = 0.028°Cm^2W^{-1}$, and $c_4 = -1.528°Csm^{-1}$ [71].

B.2.2 Wind

We calculate wind capacity factors using the formulation described in [19] for the composite 1.5 MW IEC class III turbine with power curves from the System Advisor Model (SAM) [70] as:

$$CF_{wind}^d = p(W_{100}^d) \tag{4}$$

where p is a function describing the power curve and W_{100}^d is the daily corrected 100m wind speed. The correction accounts for air density and humidity related effects on the wind turbine performance and is carried out as:

$$W_{100} = W_{10}\left(\frac{100m}{10m}\right)^{1/7} \tag{5}$$

$$W_{100} = W_{100}\left(\frac{\rho_m}{1.225}\right)^{1/3} \tag{6}$$

$$\rho_m = \rho_d\left(\frac{1 + QREFHT}{1 + 1.609 \times HUSS}\right) \tag{7}$$

$$\rho_d = \frac{PS}{\boldsymbol{R} \times (T + 273.15)} \tag{8}$$

Eqs.5 and 6 scales the 10m wind speed to 100m and correct for air density as this affects the force exerted on the turbine blades, where ρ_m is the humidity corrected air density, which is in turn derived from the surface specific humidity ($HUSS$) as shown in eq.7. ρ_d is the dry air density which is derived using the ideal gas law from surface pressure [units-Pa](PS) and surface temperature (T) as shown in eq.8, where $\boldsymbol{R} = 287.058Jkg^{-1}K^{-1}$ is the gas constant.

We estimate wind generation for all locations across WECC assuming a class-III wind turbine. The power curve from SAM is provided as the power output at discrete wind speeds (figure B.2), and we convert this into a continuous function through linear interpolation. We include the discrete power curve in this SI.

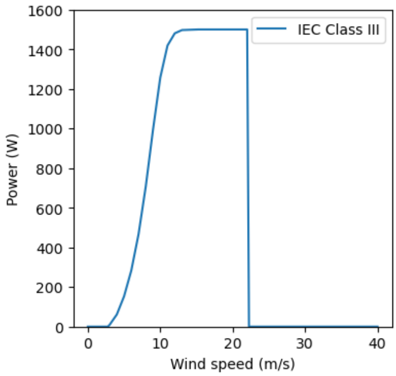

Fig. B.2: Power curve for 1.5 MW IEC class III turbine

B.3 Hydroelectricity generation

We obtain monthly hydroelectric generation forecasts using a linear regression model which predicts hydro electric generation as a function of runoff. We train the regression against cleaned plant level hydroelectric generation from the RectifHyd dataset [66] and river run-off from the ERA5-land dataset. To predict the hydro generation for each ensemble member we use the runoff data from the LENS2 dataset. Owing to the coarse resolution of the LENS2 data, and computational costs to obtain river run and reservoir flows, we build our regression models for individual "drought regions". These drought regions represent eight hydropower climatic regions for the western US, and determined using clustering techniques based on similarity of climatic conditions and reservoir characteristics [65].

We carry out the hydroelectric generation forecasting with the following steps:

1. ERA5 representation of runoff is daily accumulations at 00 hours in m/day and averaged over month, cesm is daily mean at mm/day averaged over month, so we reconcile these to the same units.
2. There is a bias between LENS2 and ERA5-Land datasets, so we bias correct LENS2 data ensemble mean to match reanalysis data for the period 1980-2020 using a scaling factor. Figure B.6 shows the bias correction factors for each drought region. The range in the figure represents the bias correction factors if we corrected each ensemble member individually rather than correcting the ensemble mean.

3. We then train our regression models to predict annual generation (for a hydrological year), using the observed hydro generation data and ERA5 surface run off. We predict annual generation based on LENS2 data and use the monthly shapes in figure B.7 to get monthly generation.
4. Figures B.8 and B.9 show predicted hydroelectric generation from all ensembles at the drought regional level and from 1 ensemble for the WECC subregions respectively.

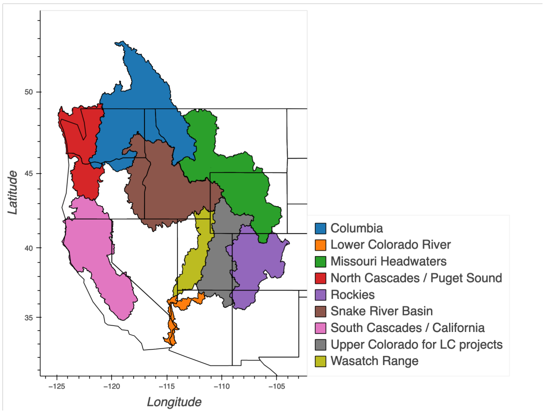

Fig. B.3: Drought regions used in the RectifHyd dataset

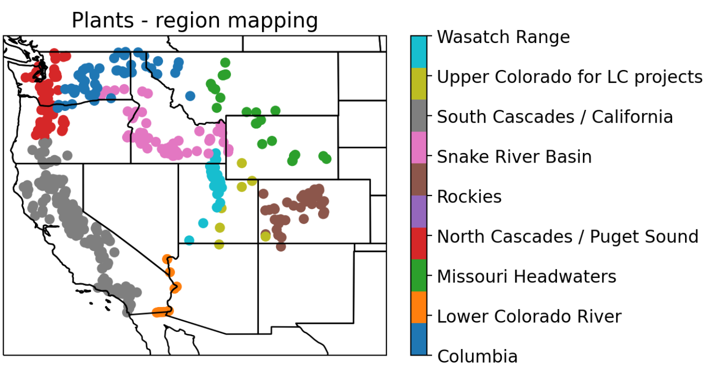

Fig. B.4: Mapping of hydropower plants in WECC to the drought regions

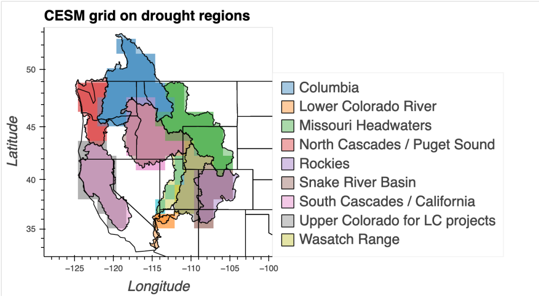

Fig. B.5: Mapping of CESM grid cells to the drought regions

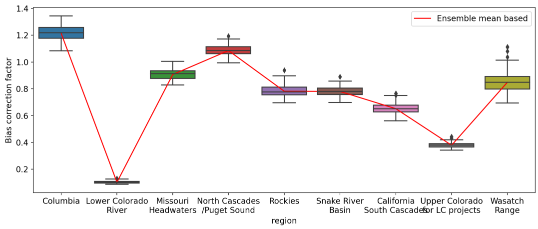

Fig. B.6: Bias correction factors for the drought regions.

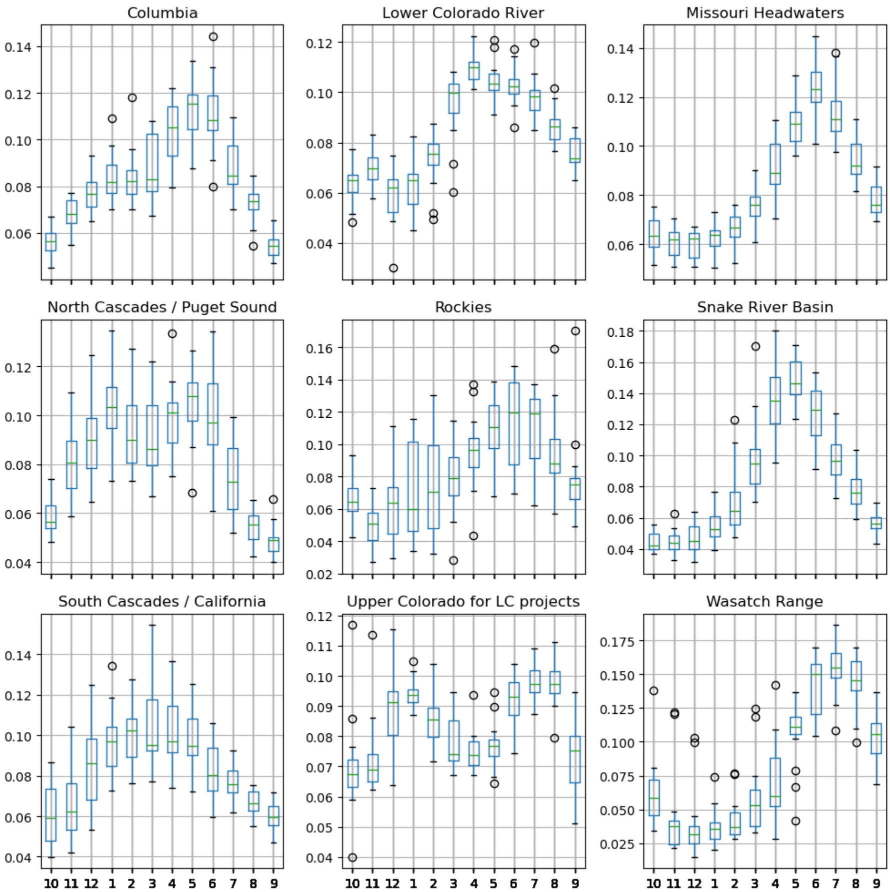

Fig. B.7: Annual to monthly disaggregation shapes

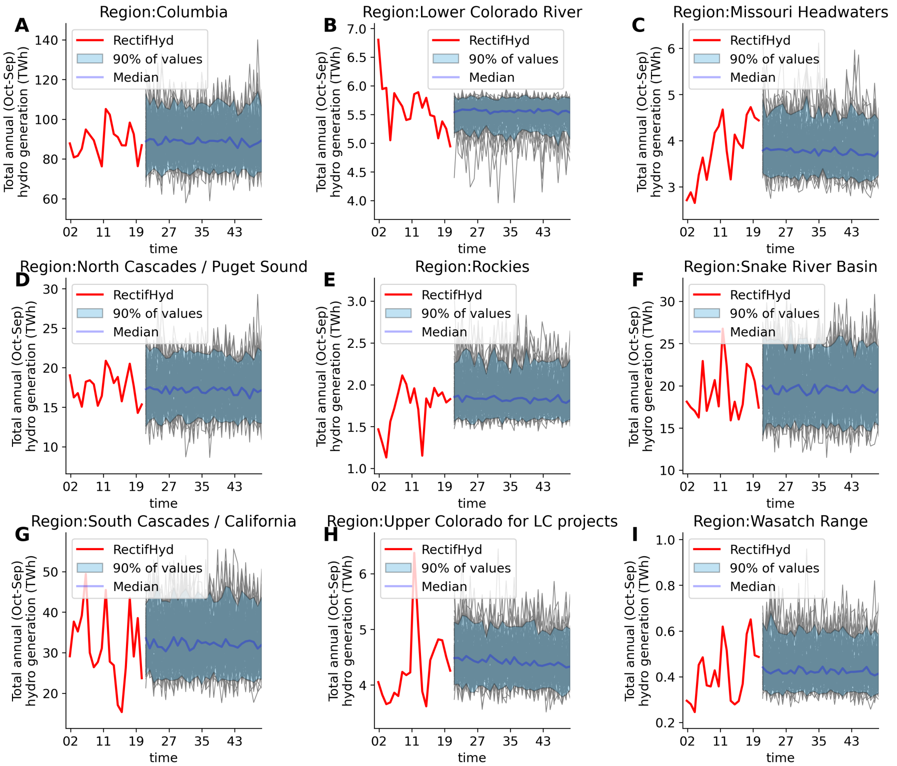

Fig. B.8: Comparison of annual hydroelectric generation from all ensembles against observations

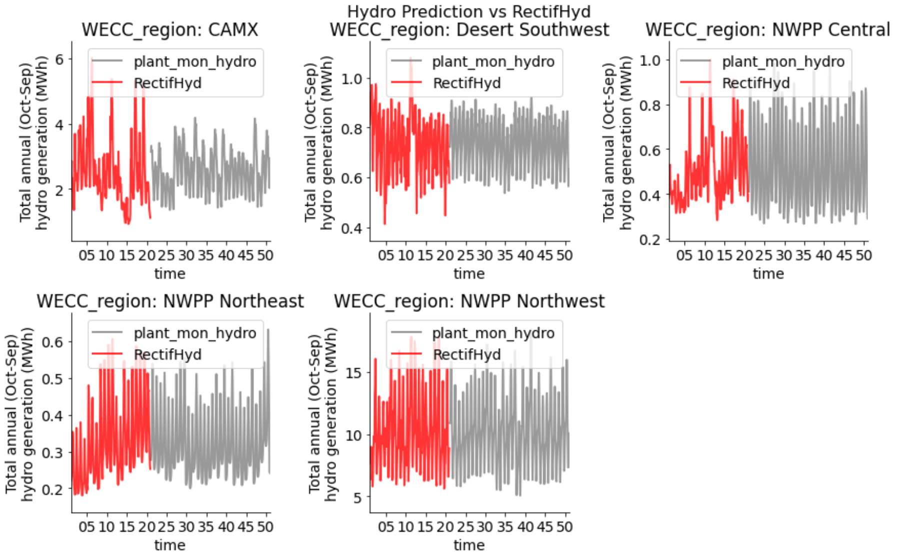

Fig. B.9: WECC subregional hydroelectric generation for the *r4i1061p1f1* ensemble

B.3.1 Driving Ensemble Parameters

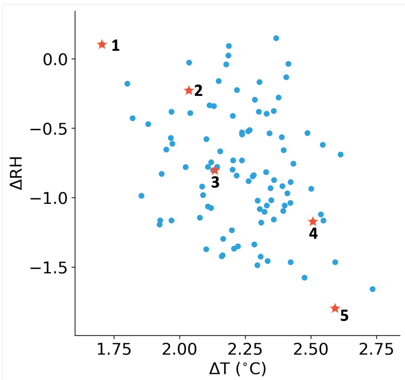

Fig. B.10: Difference between 2035-2065 and 1985-2015 climatology of surface temperature and relative humidity for the 100 CESM2-LE ensemble members. The stars show ΔT and ΔRH the ensemble members chosen for capacity expansion runs. Refer table 2 for information about the selected ensemble members.

Index	LENS2 member ID	ΔT (°C)	ΔRH
1	r12i1301p1f2	1.70	0.10
2	r10i1181p1f1	2.03	-0.22
3	r9i1301p1f1	2.13	-0.80
4	r10i1191p1f2	2.50	-1.17
5	r5i1231p1f1	2.59	-1.79

Table 2: ΔT, ΔRH, and ensemble ID of the members chosen for expansion planning. Index corresponds to star labels in Figure B.10.

Sub-region	Balancing Authorities aggregated to find demand
CAMX	CISO, BANC, TIDC, LDWP
Desert Southwest	IID, AZPS, SRP, EPE, PNM, TEPC, WALC
NWPP Central	NEVP, PACE, IPCO, PSCO
NWPP NE	WACM, NWMT, WAUW, PACE
NWPP NW	PSEI, DOPD, CHPD, AVA, TPWR, GCPD, BPAT, PGE, PACW, SCL

Table 3: Sub-region – balancing authority mapping to obtain aggregate demand

C Demand Forecasting

We derive daily subregional demand for each ensemble member using a piecewise linear regression (PLR) model [15]. The model predicts daily demand from subregional averaged daily surface temperature. We train the model with daily demand data, which is obtained by processing observed demand [72], and observed daily temperatures from ERA5. In the regression formulation we include fixed effects based on day of the week and the season. We obtain temperature bins to apply the piecewise model by splitting the subregional temperatures into 6 bins containing same number of datapoints. Because the subregions experience different temperature, we have different bins for each subregion.

C.1 Regional Demand for Electricity

The sub-regional loads are constructed by aggregating loads in smaller balancing authorities located within their boundaries [Table 3].

Subregion	Temperature Bins (°C)					
	Segment 1	Segment 2	Segment 3	Segment 4	Segment 5	Segment 6
CAMX	[0.83,8.44)	[8.44,11.72)	[11.72,15.34)	[15.34,19.52)	[19.52,24.63)	[24.63,29.82)
Desert Southwest	[-5.46,6.18)	[6.18,10.78)	[10.78,15.59)	[15.59,20.82)	[20.82,25.17)	[25.17,30.89)
NWPP Central	[-16.23,-0.94)	[-0.94,4.31)	[4.31,9.14)	[9.14,15.33)	[15.33,21.85)	[21.85,26.88)
NWPP NE	[-23.87,-5.27)	[-5.27,0.47)	[0.47,5.63)	[5.63,11.61)	[11.61,17.83)	[17.83,25.58)
NWPP NW	[-13.73,0.10)	[0.10,4.05)	[4.05,7.68)	[7.68,12.80)	[12.80,17.95)	[17.95,25.92)

Table 4: Temperature bins for piecewise linear regression by subregion.

Subregion	Coefficient corresponding to					
	Segment 1	Segment 2	Segment 3	Segment 4	Segment 5	Segment 6
CAMX	-73.38	-99.82	305.46	513.98	1038.17	1731.93
Desert Southwest	-169.99	-0.18	170.67	439.61	624.10	497.94
NWPP Central	-115.00	-158.59	-88.00	164.17	397.05	523.58
NWPP NE	-36.83	-51.61	-63.73	-6.91	97.34	154.42
NWPP NW	-406.10	-448.34	-460.85	-163.03	179.54	352.19

Table 5: Coefficients of corresponding segments from table 4

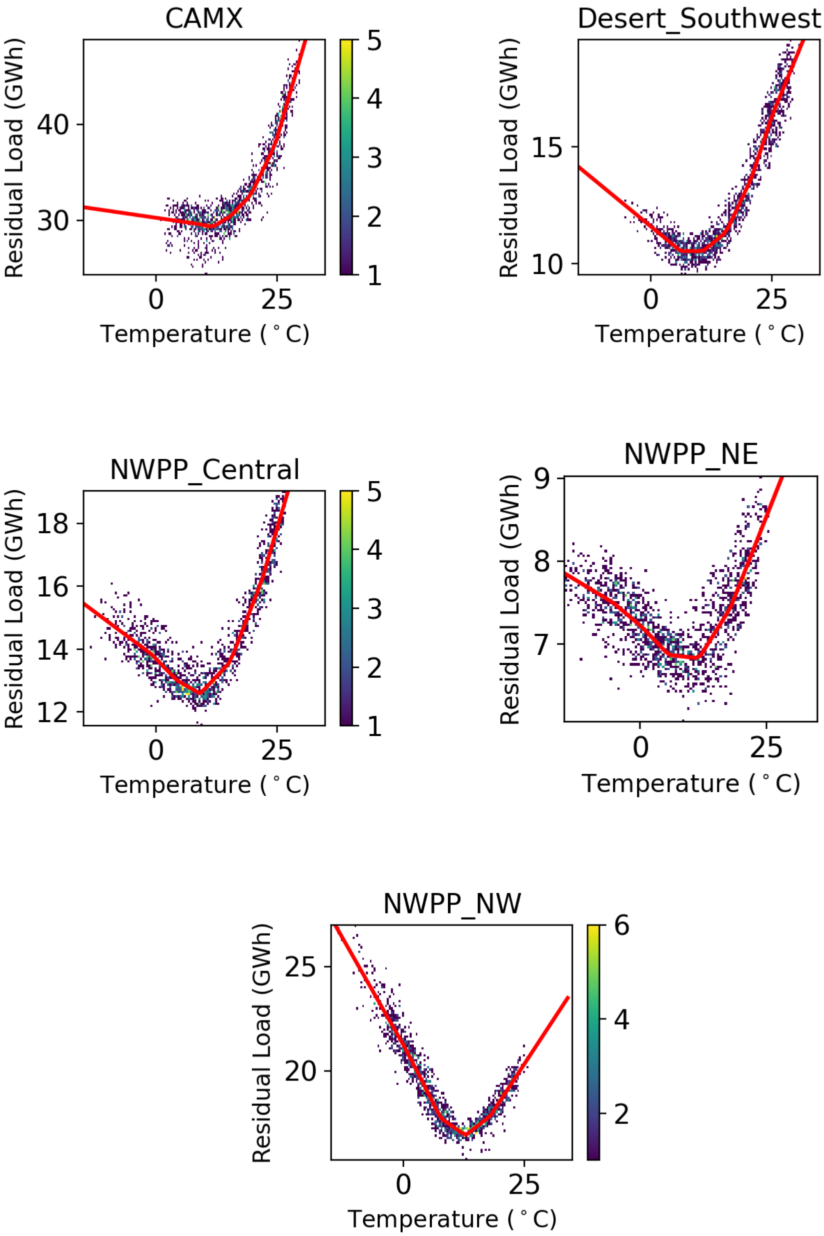

Fig. C.1: Piecewise linear regression results overlaid with observed values for residual load versus temperature in each subregion. Residual load isolates the temperature-dependent portion of load.

D Capacity Deratings and Temperature-Dependent Forced Outage Rates of Fossil-Based Thermal Power Plants

Fossil-based thermal power plants are vulnerable to capacity deratings, or reductions in available generating capacity. We estimate deratings using existing bottom-up relationships for steam turbine and combined cycle (CC) plants with recirculating or dry cooling and for combustion turbines. Deratings for plants with once through cooling are driven by water intake conditions (e.g., river temperatures) and regulations, so requires detailed hydrological modeling outside of our analytic scope. We approximate deratings of coal and CC facilities with carbon capture and sequestration (CCS) to be the same as coal and CC facilities without CCS. Deratings are calculated following the methods following Craig et al. (2020), which sources a bottom-up derating estimate for combustion turbines from Bartos and Chester (2015) and a statistical model of deratings at coal and gas STs and CCs from Loew et al. (2018). In these relationships, CT deratings are a function of surface air temperatures; STs and CCs with recirculating cooling (RC) are a function of surface air temperatures and relative humidity; and STs and CCs with dry cooling (DC) are a function of surface air temperatures and surface air pressure. RC and DC facilities have varying designs, which in turn have varying vulnerabilities to thermal deratings. Data on RC and DC designs is not publicly available, so we assume RC and DC designs that are moderately resilient against deratings. Specifically, we assume a RC design of inlet and outlet cooling water temperatures of 75 and 95 degrees F, respectively, and a DC design with an initial temperature difference of 45 degrees F. We obtain cooling types by power plant from EIA Form 860.

We calculate temperature-dependent forced outage rates for thermal power plants using the best available plant-type-specific relationships from existing literature [67].

Table 6: Temperature dependent forced outage rates of different generators from Murphy et al. (2019).

Closest temperature value [$°C$]	**-15**	**-10**	**-5**	**0**	**5**	**10**	**15**	**20**	**25**	**30**	**35**
Nuclear	1.9 %	1.8 %	1.7 %	1.8 %	1.9 %	2.1 %	2.7 %	3.1 %	3.9 %	6.6 %	12.4 %
Combined cycle gas	14.9 %	8.1 %	4.8 %	3.3 %	2.7 %	2.5 %	2.8 %	3.5 %	3.5 %	4.1 %	7.2 %
Simple cycle gas	19.9 %	9.9 %	5.1 %	3.1 %	2.4 %	2.2 %	2.4 %	2.7 %	3.1 %	3.9 %	6.6 %
Steam turbine coal	13.3 %	11.2 %	9.9 %	9.1 %	8.6 %	8.3 %	8.4 %	8.6 %	9.4 %	11.4 %	14. %
Hydro	7 %	4.3 %	3.2 %	2.7 %	2.6 %	2.6 %	2.7 %	2.7 %	2.5 %	2.9 %	8.2 %
Solar, wind, storage, other	5 %	5 %	5 %	5 %	5 %	5 %	5 %	5 %	5 %	5 %	5 %

E Capacity Expansion Model

The capacity expansion (CE) model optimizes new capacity investments, operations of new and existing units, and inter-regional electricity transfers by minimizing total system costs subject to system and unit-level constraints. Total system costs equal the sum of the cost of electricity generation of existing and new units and the cost of new capacity investments. Electricity generation costs equal the sum of fixed operations and maintenance (O&M) costs and variable electricity generation costs, which include fuel costs and variable O&M costs. The model runs from 2023 to 2040 in 2-year time steps. In each model run, the CE model can build natural gas combined cycle (NGCC), wind, and solar generators, and can build coal or NGCC with carbon capture and sequestration (CCS) beginning in 2031 given the current immature state of the technology. We obtain overnight capital costs and fixed and variable operation and maintenance (O&M) costs for each time step from NREL's Annual Technology Baseline (ATB) moderate technology development scenario [73].

The CEM model divides WECC into five regions; inter-regional transmission and capacity investments are optimized between regions, and supply and demand are balanced within each region (accounting for imports and exports).

To reflect ongoing scale up of wind and solar investment potential, we include a WECC-wide limit on wind and solar investments in each time step. Annual limits begin in the first model run (2023-2024) at 5.2 and 6.8 GW for wind and solar, respectively, or double the maximum annual capacity additions in recent years (2020-2022) since our model runs in 2-year time steps. Maximum potential wind and solar investments grow through 2040 at a compounding annual growth rate of 0.3. In addition to WECC-wide investment limits on wind and solar, we capture local limits on capacity investments following methods outlined by Wu et al. [74]. In general, we exclude developable area on the basis of environmental, techno-economic, land use, and legal criteria. Exclusions include Bureau of Land Management (BLM) exclusions; United States Geologic Service protected areas; airports; lakes; mines; military areas; census urban zones; flood zones; high slopes; and high population densities. After accounting for exclusions, we sum available area for wind or solar deployment by CESM2 grid cell, convert area to installed capacity using wind and solar densities of 0.9 and 5.7 W per square meter [75], respectively, and optimize wind and solar investments at the grid cell level.

E.1 Functional Forms

E.1.1 Parameters and Variables

Parameter	Definition	Unit
P_i^{MAX}	Maximum power rating of existing unit i	MW
P_c^{MAX}	Maximum power rating of new unit c	MW
P_l^{MAX}	Maximum transmission capacity of line l	MW
FOM_c	Fixed O&M cost of new unit c	\$/MW/year
OCC_c	Overnight capital cost of new unit c	\$/MW
OCC_l	Overnight capital cost of transmission expansion along line l	\$/MW
CRF_c	Capital recovery factor of new unit c	\$/MW
CRF_l	Capital recovery factor of new transmission line l	\$/MW
OC_c	Operational cost of new unit c	\$/MWh
VOM_c	Variable O&M cost of new unit c	\$/MWh
VOM_i	Variable O&M cost of existing unit i	\$/MWh
OC_i	Operational cost of existing unit i	\$/MWh
OC_c	Operational cost of new unit c	\$/MWh
FC_c	Fuel cost of new unit c	\$/MMBtu
FC_i	Fuel cost of existing unit i	\$/MMBtu
HR_c	Heat rate of new unit c	MMBtu/MWh
HR_i	Heat rate of existing unit i	MMBtu/MWh
$ER_i^{CO_2}$	CO_2 emissions rate of existing unit i	ton/MMBtu
$ER_c^{CO_2}$	CO_2 emissions rate of new unit c	ton/MMBtu
R	Discount rate = 0.07	–
LT_c	Life time of new units c	Years
$N_{c_r}^{MAX}$	Maximum capacity of new wind or solar units c built	MW
$P_{c_r}^{WECC,MAX}$	Maximum number of total renewable capacity c_r built WECC-wide	MW
$D_{z,t}$	Total load (or electricity demand) in region z at time t	MWh
D_t	Total load (or electricity demand) across regions at time t	MWh

Table 7: List of Parameters

Parameter	Definition	Unit
$P_{t,z}^{MAX,WIND}$	Maximum aggregate wind profile in region z at time t	MW
$P_{t,z}^{MAX,SOLAR}$	Maximum aggregate solar profile in region z at time t	MW
$H_{b,z}$	Maximum hydropower generation in region z and month b	MWh
$FOR_{i,t}$	Forced outage rate of existing unit i at time t	–
$DR_{i_{th},t}$	Capacity derate of existing thermal CT, CC, or coal plants i_{th} at time t	–
$DR_{c_{th},t}$	Capacity derate of new thermal CC or coal plants c_{th} at time t	–
FOR_t^{RE}	Forced outage rate of existing wind and solar units at time t	–
$FOR_{c,t}$	Forced outage rate of new unit c at time t	–
$E_{CO_2}^{MAX}$	WECC-wide carbon dioxide emissions cap	tons
$CF_{c_r,t}$	Capacity factor of new renewable unit c_r at time t	–
RL_i	Maximum ramp rate of existing unit i	MW
RL_c	Maximum ramp rate of new unit c	MW
ν	Transmission losses per unit of electricity transferred between regions	%

Table 7: List of Parameters (Continued)

Set	Definition	Index	Note
$\mathbb{C}$	Set of potential new units	c	–
$\mathbb{C}_z$	Set of potential new units in region z	c_z	$\mathbb{C}_z \in \mathbb{C}$
$\mathbb{C}_r$	Set of potential new renewable units	c_r	$\mathbb{C}_r \in \mathbb{C}$
$\mathbb{C}_{th}$	Set of potential new coal or NGCC thermal units	c_{th}	$\mathbb{C}_{th} \in \mathbb{C}$
$\mathbb{I}$	Set of existing units	i	–
$\mathbb{I}_z$	Set of existing units in region z	i_z	$\mathbb{I}_z \in \mathbb{I}$
$\mathbb{I}_r$	Set of existing renewable units	i_r	$\mathbb{I}_r \in \mathbb{I}$
$\mathbb{I}_{th}$	Set of existing CT, CC, or coal thermal units	i_{th}	$\mathbb{I}_{th} \in \mathbb{I}$
$\mathbb{I}_w$	Set of existing wind units	i_w	$\mathbb{I}_w \in \mathbb{I}$
$\mathbb{I}_{w_z}$	Set of existing wind units in region z	i_{w_z}	$\mathbb{I}_{w_z} \in \mathbb{I}_w$
$\mathbb{I}_o$	Set of existing solar units	i_o	$\mathbb{I}_o \in \mathbb{I}$
$\mathbb{I}_{o_z}$	Set of existing solar units in region z	i_{o_z}	$\mathbb{I}_{o_z} \in \mathbb{I}_o$
$\mathbb{L}$	Set of transmission lines	l	–
$\mathbb{L}_z^{OUT}$	Set of transmission lines flowing out of region z	l_z^{OUT}	$\mathbb{L}_z^{OUT} \in \mathbb{L}$
$\mathbb{L}_z^{IN}$	Set of transmission lines flowing into region z	l_z^{IN}	$\mathbb{L}_z^{IN} \in \mathbb{L}$
$\mathbb{B}$	Set of months	b	–
$\mathbb{T}$	Set of days	t	–
$\mathbb{T}_p$	Set of peak demand day	t_p	$\mathbb{T}_p \in \mathbb{T}$
$\mathbb{Z}$	Set of regions in WECC	z	–

Table 8: List of Sets

Variable	Definition	Unit
n_c	Number of new units built of type c	Positive number
n_l	Total new transmission line capacity investments in line l	MW
$p_{i,t}$	Electricity generation from existing unit i at time t	MWh
$p_{c,t}$	Electricity generation from new unit c at time t	MWh
$f_{l,t}$	Total electricity flow in line l at time t	MWh

Table 9: List of Variables

E.2 Objective Function

The CE model's objective function minimizes total annual fixed plus variable costs, where fixed costs capture investment costs in new transmission and electricity generators, and variable costs capture operational costs of new and existing generators:

$$
\begin{aligned}
TC^{CE} = &\left[\sum_c n_c \times P_c^{MAX} \times (FOM_c + OCC_c \times CRF_c)\right] \\
&+ \left[\sum_l n_l \times OCC_l \times CRF_l\right] + \left[\sum_t \left(\sum_c p_{c,t} \times OC_c + \sum_i p_{i,t} \times OC_i\right)\right],
\end{aligned}
$$

$$\forall i \in \mathbb{I},\, c \in \mathbb{C},\, l \in \mathbb{L} \tag{9}$$

where c indexes potential new units; t indexes time intervals (days); i indexes existing units; l indexes potential new transmission lines; n_c is number of new unit investments; n_l is total new transmission line capacity investments in line l (MW); P^{MAX} is maximum capacity of unit (MW); FOM is fixed operation and maintenance (O&M) costs of units ($/MW/year); OCC is overnight capital cost of new investments ($/MW); CRF is capital recovery factor; p_c is electricity generation from new unit c (MWh); p_i is electricity generation from existing unit i (MWh); and OC is operational costs of new or existing units ($/MWh). OC is defined for new and existing generators as:

$$OC_i = VOM_i + HR_i \times FC_i \qquad \forall i \in \mathbb{I}, \tag{10a}$$

$$OC_c = VOM_c + HR_c \times FC_c \qquad \forall c \in \mathbb{C} \tag{10b}$$

where VOM is variable O&M costs ($/MWh), HR is heat rate (MMBtu/MWh), and FC is fuel cost ($/MMBtu). CRF_c is defined as:

$$CRF_c = \frac{R}{1 - \dfrac{1}{(1+R)^{LT_c}}} \qquad \forall c \in \mathbb{C}, \tag{11}$$

where R is discount rate and LT is plant lifetime (years).

E.3 System-level Constraints

The CE model requires total adjusted capacity to meet peak annual demand on a WECC-wide basis:

$$\begin{aligned} D_t \quad \leq \quad & \sum_{c_{th} \in C_{th}} P^{MAX}_{c_{th}} \times (1 - FOR_{c_{th},t}) \times (1 - DR_{c_{th},t}) \times n_{c_{th}} \\ & + \sum_{c_r \in C_r} P^{MAX}_{c_r} \times (1 - FOR_{c_r,t}) \times n_{c_r} \times CF_{c_r,t} \\ & + \sum_{i \in (I - I_W - I_O - I_{TH})} (1 - FOR_{i,t}) \times P^{MAX}_i \\ & + \sum_{i_{th} \in I_{TH}} (1 - FOR_{i_{th},t}) \times (1 - DR_{i_{th},t}) \times P^{MAX}_{i_{th}} \\ & + \sum_{z} \left(P^{MAX,SOLAR}_{z,t} + P^{MAX,WIND}_{z,t} \right) \times (1 - FOR^{RE}_t), \\ & \forall t \in \mathbb{T}_p \end{aligned} \tag{12}$$

where c_{th} and c_r index new thermal and renewable plant types, respectively; i_w and i_o index existing wind and solar generators, respectively;

z indexes regions; FOR is forced outage rate; CF is capacity factor; $P^{MAX,SOLAR}$ is maximum regional generation by existing solar generators (MWh); $P^{MAX,WIND}$ is maximum regional generation by existing wind generators (MWh); and T_p indicates the annual peak demand day. Adjusted capacity here accounts for temperature-dependent forced outage rates of generators [Table 6] and daily capacity factors for wind and solar facilities. Note that this PRM is enforced across all of WECC rather than on a region-by-region basis.

The CE model also requires supply balance demand at each time step:

$$D_{z,t} + \sum_{l_z^{OUT} \in \mathbb{L}_z^{OUT}} f_{l_z^{OUT},t} \leq \begin{array}{l} \sum_{i_z \in \mathbb{I}_z} p_{i_z,t} + \sum_{c_z \in \mathbb{C}_z} p_{c_z,t} \\ + \sum_{l_z^{IN} \in \mathbb{L}_z^{IN}} f_{l_z^{IN},t} \times \nu, \quad \forall z \in \mathbb{Z}, t \in \mathbb{T}, \end{array} \tag{13}$$

where z indexes zones, l indexes transmission lines, i_z indexes existing units in region z, c_z indexes new units in region z, l_z^{IN} indexes lines flowing out of region z, l_z^{OUT} indexes transmission lines flowing out of region z, ν indicates losses for each unit of electricity imported into a region (assumed to be 5%), and f is electricity flows along transmission lines.

The total electricity flow through a transmission line ($f_{l,t}$) cannot exceed the line's initial transmission capacity (P_l^{MAX}) plus new capacity investments (n_l):

$$f_{l,t} \leq P_l^{MAX} + n_l, \quad \forall l \in \mathbb{L}, \, t \in \mathbb{T}, \tag{14}$$

where l indexes transmission lines, and $f_{l,t}$ is total electricity flow in line l at time t (MWh).

To examine power systems that meet alternative decarbonization targets, we enforce four different CO_2 emission caps ($E_{CO_2}^{MAX}$ on WECC-wide emissions:

$$E_{CO_2}^{MAX} \geq \left[\sum_t \left(\sum_i p_{i,t} \times HR_i \times ER_i^{CO_2} + \sum_c p_{c,t} \times HR_c \times ER_c^{CO_2} \right) \right], \\ \forall t \in \mathbb{T}, \, \forall i \in \mathbb{I}, \, \forall c \in \mathbb{C} \tag{15}$$

where ER^{CO_2} is CO_2 emission rate (ton/MMBtu).

As detailed above, we enforce a WECC-wide cap on wind and solar investments ($P_{c_r}^{WECC,MAX}$) (MW) to reflect scaling up of both industries:

$$\sum_{c_r} n_{c_r} \times P_{c_r}^{MAX} \leq P_{c_r}^{WECC,MAX}, \quad \forall c_r \in \mathbb{C}_r \tag{16}$$

where n_{c_r} equals investment in new wind or solar plants.

E.4 Unit-level Constraints

E.4.1 Investment constraints

As explained above, the CE model places an upper bound on wind and solar investments by grid cell based on the area of each grid cell; restrictions on development based on technoeconomic, legal, environmental, and land-use criteria; and the energy density of wind and solar:

$$0 \le n_{c_r} \times P^{MAX}_{c_r} \le N^{MAX}_{c_r}, \quad \forall c_r \in \mathbb{C}_r \tag{17}$$

where n_{c_r} equals investment in new wind or solar plants and $N^{MAX}_{c_r}$ equals the maximum investment in new wind or solar plants by grid cell. Existing wind and solar capacities are subtracted from the grid cell's maximum capacity in calculating $N^{MAX}_{c_r}$.

E.4.2 Generation constraints

For existing generators, electricity generation is limited by the generators' capacities:

$$0 \le p_{i,t} \le P^{MAX}_{i}, \quad \forall t \in \mathbb{T}, \, i \in \mathbb{I} \tag{18}$$

Thermal plants are vulnerable to deratings at certain ambient air temperatures. We account for deratings of combustion turbines, NGCCs, and coal-fired power plants across space and time (Section SI.D) and limit their daily generation to their derated capacity as follows:

$$p_{i_{th},t} \le DR_{i_{th},t} \times P^{MAX}_{i_{th}}, \quad \forall t \in \mathbb{T}, \, i_{th} \in \mathbb{I}_{\approx\approx} p_{c_{th},t} \le n_{c_{th}} \times DR_{c_{th},t} \times P^{MAX}_{c_{th}}, \quad \forall t \in \mathbb{T}, \, c \tag{19a}$$

Combined electricity generation by existing wind and solar generators is limited to aggregate wind and solar generation profiles:

$$\sum_{i_{w_z} \in \mathbb{I}_{w_z}} p_{i_{w_z},t} \le P^{MAX,WIND}_{z,t}, \quad \forall t \in \mathbb{T}, z \in \mathbb{Z}, \tag{20a}$$

$$\sum_{i_{o_z} \in \mathbb{I}_{o_z}} p_{i_{o_z},t} \le P^{MAX,SOLAR}_{z,t}, \quad \forall t \in \mathbb{T}, z \in \mathbb{Z}, \tag{20b}$$

New generators' electricity generation cannot exceed their new capacity investments:

$$0 \le p_{c,t} \le n_c \times P^{MAX}_{c}, \quad \forall t \in \mathbb{T}, \, c \in \mathbb{C} \tag{21}$$

Electricity generation by new renewable generators is also constrained by site-specific capacity factor timeseries:

$$p_{c_r,t} \leq n_{c_r} \times P_{c_r}^{MAX} \times CF_{c_r,t}, \quad \forall t \in \mathbb{T},\, c_r \in \mathbb{C}_r \tag{22}$$

Hydropower generation is constrained based on observed data for each of our weather years. Since we ignore transmission constraints within each of our five regions, we aggregate hydropower capacity by region, then limit total hydropower generation by month (or time block):

$$\sum_{t_b \in T_b, i_{h_z} \in I_{h_z}} p_{i_{h_z},t_b} \leq H_{b,z}, \forall z \in \mathbb{Z}, b \in \mathbb{B} \tag{23}$$

where i_{h_z} indexes all hydropower units in region z and $H_{b,z}$ equals maximum total hydropower generation in month b and region z [**??**].

The CE model places an upper bound on upwards changes in electricity generation from one time period to the next, i.e. in upward ramps, for new and existing units:

$$p_{i,t_b} - p_{i,t_b-1} \leq RL_i, \quad \forall t_b > 1, i \in \mathbb{I} \tag{24a}$$

$$p_{c,t_b} - p_{c,t_b-1} \leq n_c \times P_c^{MAX} \times RL_c \quad \forall t_b > 1, c \in \mathbb{C} \tag{24b}$$

where RL equals the ramp limit. We only constrain upwards ramps for two reasons: (1) downward ramps can be more easily achieved through curtailment of renewables than upwards ramps and (2) for computational tractability.

E.5 Data

In this section, we discuss the data and intermediate steps to calculate the parameters that are used in the model.

E.5.1 Regional Demand for Electricity

The sub-regional loads are constructed by aggregating loads in smaller balancing authorities located within their boundaries per the following table.

E.5.2 Generator Fleet

Initial Generator Fleet

To construct our 2022 initial representative existing generator fleet, we begin with unit-level data on active existing units from *The National Electric Energy Data System* (NEEDS) dataset version 6 (updated in February 2023) [**?**]. Because NEEDS lacks several parameters needed in our CE model, we merge the NEEDS dataset with EIA860 dataset [**?**] and add carbon dioxide (CO_2) emission rates from the the U.S. Energy Information Administration (EIA)'s *Carbon Dioxide Emissions Coefficients* [**?**], fuel prices from EIA's *Annual*

Sub-region	CC gas	OC gas	Hydro	Nuclear	Coal	Solar	Wind	Other
CAMX	20641	10825	10147	0	17	10644	5764	4010
Desert Southwest	11256	4855	3840	3937	5333	2303	1488	363
NWPP Central	10486	5053	954	0	6693	3128	3636	1045
NWPP NE	94	465	3493	0	6562	40	2906	23
NWPP NW	6619	1669	32091	1180	0	356	6568	557

Table 10: Initial generator fleet capacity of each generator type (in MW) across the subregions. CC indicates combined cycle; OC open cycle; and coal plants are steam turbine plants.

Energy Outlook 2023, Table 3. Energy Prices by Sector and Source [**?**], and variable operation and maintenance (O&M) costs from [73]. We isolate generators within WECC, our study region, using shape files of balancing areas within WECC from NREL's ReEDS model [76]. Our initial generator fleet is described in the table 10. The *other* type of generators in the table below include geothermal, different types of waste, biomass, and other small fossil generators, which are all modeled as dispatchable capacity in the CEM and RAM.

Generator Fleet Compression

Because the existing generation fleet in WECC is large with over 4,500 units, we combine (or aggregate) existing small generators into larger generators for computational tractability. We aggregate generators within the same region using two steps and several criteria. First, for each fuel type and plant type with zero marginal costs, we aggregate all generators into a single generator by region. Zero marginal cost generators include all geothermal, wind, solar, landfill gas, municipal solid waste, biomass, and non-fossil waste generators. Second, for each fuel type and plant type with non-zero marginal costs, we aggregate generators based on age and heat rate to preserve heterogeneity in operational costs. These non-zero marginal cost units include distillate fuel oil, natural gas combined cycle, natural gas combustion turbine, residual fuel oil, and coal (including bituminous, sub-bituminous, and lignite) generators. Specifically, by region, plant type, and fuel type, we divide generators into 4 heat rate blocks, then aggregate generators together within each heat rate block by decade between 1975 and 2026. We aggregate generators up to 200 MW in size in this manner, and create combined generators of up to 10,000 MW. These size thresholds significantly reduce the size of the generator fleet while still individually modeling mid- to large-sized power plants. Heat rates and CO_2 emission rates of the aggregated generators equal the capacity-weighted heat rates and CO_2 emission rates of their constituent generators.

Transmission Capacity between	Total Capacity (GW)	Expansion Cost (1000$/MW)
NWPP-NW and NWPP-NE	12.3	474
NWPP-NW and CAMX	7.1	1,018
NWPP-NW and NWPP-Central	1.5	569
NWPP-NE and NWPP-Central	6.0	431
CAMX and Desert Southwest	3.0	1,070
CAMX and NWPP-Central	4.6	816
Desert Southwest and NWPP-Central	5.6	348

Table 11: Transmission Networks within WECC

E.5.3 System Topology

Our resource adequacy (RA) model uses the five regions that WECC uses to quantify resource adequacy in WECC [59]: NWPP NW, NWPP NE, CAMX, Desert Southwest, and NWPP Central [see figure E.1]. To align regions between the CE and RA models, we model these same five regions in our CE model.

Within each of these regions, we ignore transmission constraints. Between regions, we enforce transmission constraints. Given the lack of data regarding transmission constraints between our WECC resource adequacy regions, we estimate inter-regional transmission constraints using data from the National Renewable Energy Laboratory (NREL) Regional Energy Deployment System (ReEDS) model. ReEDS provides transmission constraints between 35 balancing areas across WECC. We assign each balancing area to a region using spatial overlays, then set transmission constraints between each pair of regions as the sum of transmission constraints between each pair of balancing areas within each region. Using this method, we identify seven inter-regional, bi-directional transmission constraints. For each of these seven inter-regional transmission constraints, we limit daily inter-regional electricity transfers to an upper capacity bound.

In addition to enforcing existing transmission constraints, the CE model can also invest in new transmission capacity between each of the seven inter-regional transmission interfaces identified above. Similar to other macro-scale planning models [77], we assume costs scale linearly with new transmission capacity, allowing us to maintain a computationally tractable linear program (LP). Per-MW costs of transmission expansion equal the distance (in miles) between the two centroids of interconnected regions times the per MW-mile cost of each bi-directional transmission line. We estimate this cost as the median of costs between each pair of balancing authorities between regions, which is taken from NREL's ReEDS Model's open access github [76]. Table 11 depicts all possible combinations of aggregate links between our five load regions and their respective aggregate capacities and total cost per MW.

E.6 WECC subregions

E.7 Model Code and Data Availability

CEM code and data are available at https://github.com/atpham88/US-CE.

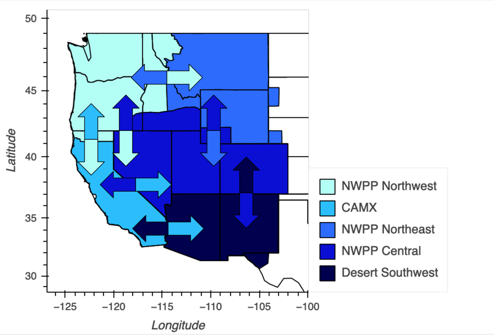

Fig. E.1: WECC subregions used in the CEM and RAM. Arrows show transmission flows between the subregions.

F Economic Dispatch Model

To calculate daily SAC and ENS, we run an economic dispatch model (EDM) for each decarbonization pathway output by our capacity expansion model in 2030 and 2040. The EDM minimizes the sum of operating, CO_2 emission, inter-regional transmission, and ENS costs by optimizing generation, inter-regional transmission, and ENS decision variables. Our EDM divides WECC into the same five regions as our CEM; inter-regional transmission and capacity investments are optimized between regions, and supply and demand are balanced within each region (accounting for imports and exports). For computational tractability, the EDM aggregates geothermal, waste, biomass, and other small fossil plants of small capacities within each plant type together (these plant types are denoted as *other* plant type in our results).

F.1 Functional Forms

F.1.1 Parameters and Variables

F.2 Objective Function

The EDM model's objective function is:

$$TC^{EDM} = \sum_{i,t} p_{i,t} \times (OC_i + HR_i \times ER_i^{CO_2} \times CP) + \sum_{z,t} ens_{z,t} \times CENS + \sum_{l,t} f_{l,t} \times FLC \qquad \forall i \in \mathbb{I},\, l \in \mathbb{L},\, z \in \mathbb{Z} \tag{25}$$

where t indexes time intervals (days); i indexes existing units; l indexes transmission lines; z indexes regions; p is electricity generation (MWh); OC is operational cost ($/MWh); HR is heat rate (MMBtu/MWh); ER is CO_2 emissions rate (ton/MMBtu); CP is CO_2 emissions price ($/ton); ens is energy not served (MWh); $CENS$ is cost of energy not served ($/MWh); FLC is the

Parameter	Definition	Unit
P_i^{MAX}	Maximum power rating of existing unit i	MW
P_l^{MAX}	Maximum transmission capacity of line l	MW
VOM_i	Variable O&M cost of existing unit i	\$/MWh
OC_i	Operational cost of existing unit i	\$/MWh
FC_i	Fuel cost of existing unit i	\$/MMBtu
HR_i	Heat rate of existing unit i	MMBtu/MWh
$ER_i^{CO_2}$	CO_2 emissions rate of existing unit i	ton/MMBtu
CP	CO_2 emissions price	\$/ton
$D_{z,t}$	Total load (or electricity demand) in region z at time t	MWh
$P_{t,z}^{MAX,WIND}$	Maximum aggregate wind profile in region z at time t	MW
$P_{t,z}^{MAX,SOLAR}$	Maximum aggregate solar profile in region z at time t	MW
$H_{b,z}$	Maximum hydropower generation in region z and month b	MWh
$FOR_{i,t}$	Forced outage rate of existing unit i at time t	–
$DR_{i,t}$	Capacity derate of existing unit i at time t	–
$CENS$	Cost of energy not served	\$/MWh
FLC	Cost of electricity flows between regions	\$/MWh

Table 12: List of Parameters (Continued)

Set	Definition	Index	Note
$\mathbb{I}$	Set of existing units	i	–
$\mathbb{I}_z$	Set of existing units in region z	i_z	$\mathbb{I}_z \in \mathbb{I}$
$\mathbb{I}_r$	Set of existing renewable units	i_r	$\mathbb{I}_r \in \mathbb{I}$
$\mathbb{I}_w$	Set of existing wind units	i_w	$\mathbb{I}_w \in \mathbb{I}$
$\mathbb{I}_{w_z}$	Set of existing wind units in region z	i_{w_z}	$\mathbb{I}_{w_z} \in \mathbb{I}_w$
$\mathbb{I}_o$	Set of existing solar units	i_o	$\mathbb{I}_o \in \mathbb{I}$
$\mathbb{I}_{o_z}$	Set of existing solar units in region z	i_{o_z}	$\mathbb{I}_{o_z} \in \mathbb{I}_o$
$\mathbb{L}$	Set of transmission lines	l	–
$\mathbb{L}_z^{OUT}$	Set of transmission lines flowing out of region z	l_z^{OUT}	$\mathbb{L}_z^{OUT} \in \mathbb{L}$
$\mathbb{L}_z^{IN}$	Set of transmission lines flowing into region z	l_z^{IN}	$\mathbb{L}_z^{IN} \in \mathbb{L}$
$\mathbb{B}$	Set of months	b	–
$\mathbb{T}$	Set of days	t	–
$\mathbb{Z}$	Set of regions in WECC	z	–

Table 13: List of Sets

Variable	Definition	Unit
$p_{i,t}$	Electricity generation from existing unit i at time t	MWh
$ens_{z,t}$	Energy not served in region z at time t	MWh
$f_{l,t}$	Total electricity flow in line l at time t	MWh

Table 14: List of Variables

cost of electricity flows between regions (\$/MWh); and f is electricity flows between regions (MWh). The $CENS$ is set large enough to be the energy of last resort in the model (or \$1000 per MWh), while the FLC is set to \$1/MWh to incentivize balancing within regions before relying on imports or exports. OC is defined as:

$$OC_i = VOM_i + HR_i \times FC_i \qquad \forall i \in \mathbb{I} \tag{26}$$

where VOM is variable O&M costs (\$/MWh) and FC is fuel cost (\$/MMBtu).

F.3 Constraints

The EDM requires supply balance demand at each time step in each region:

$$D_{z,t} + \sum_{l_z^{OUT} \in \mathbb{L}_z^{OUT}} f_{l_z^{OUT},t} \quad \leq \quad \sum_{i_z \in \mathbb{I}_z} p_{i_z,t} + \sum_{l_z^{IN} \in \mathbb{L}_z^{IN}} f_{l_z^{IN},t} \times \nu, \quad \forall z \in \mathbb{Z}, t \in \mathbb{T}, \tag{27}$$

where i_z indexes existing units in region z, l_z^{IN} indexes lines flowing out of region z, l_z^{OUT} indexes transmission lines flowing out of region z, and f is electricity flows along transmission lines.

The total electricity flow through a transmission line ($f_{l,t}$) cannot exceed the line's transmission capacity (P_l^{MAX}):

$$f_{l,t} \leq P_l^{MAX}, \quad \forall l \in \mathbb{L}, \, t \in \mathbb{T}, \tag{28}$$

where l indexes transmission lines, and $f_{l,t}$ is total electricity flow in line l at time t (MWh).

Electricity generation by each generator is limited by its capacity derated to account for thermal deratings (DR) when relevant and for forced outage rates (FOR):

$$p_{i,t} \leq (1 - DR_{i,t}) \times (1 - FOR_{i,t}) \times P_i^{MAX}, \quad \forall t \in \mathbb{T}, \, i \in \mathbb{I} \tag{29a}$$

We account for thermal deratings for combustion turbines, NGCCs, and coal-fired power plants, and FORs for all generators (Section SI.D). FORs are applied for all units; wind and solar are assumed to have a 5% FOR, while all other units have temperature-dependent forced outage rates (Section SI.D).

Combined electricity generation by wind and solar generators is limited to aggregate wind and solar generation profiles derated by a forced outage rate (FOR) set to 5%:

$$\sum_{i_{w_z} \in \mathbb{I}_{w_z}} p_{i_{w_z},t} \leq P_{z,t}^{MAX,WIND} \times (1 - FOR), \quad \forall t \in \mathbb{T}, z \in \mathbb{Z}, \tag{30a}$$

$$\sum_{i_{o_z} \in \mathbb{I}_{o_z}} p_{i_{o_z},t} \leq P_{z,t}^{MAX,SOLAR} \times (1 - FOR), \quad \forall t \in \mathbb{T}, z \in \mathbb{Z}, \tag{30b}$$

Hydropower generation is constrained based on observed data for each of our weather years. Since we ignore transmission constraints within each of our five regions, we aggregate hydropower capacity by region, then limit total hydropower generation by month (or time block):

$$\sum_{t_b \in T_b, i_{h_z} \in I_{h_z}} p_{i_{h_z},t_b} \leq H_{b,z}, \forall z \in \mathbb{Z}, b \in \mathbb{B} \tag{31}$$

where i_{h_z} indexes all hydropower units in region z and $H_{b,z}$ equals maximum total hydropower generation in month b and region z.

F.4 Model Code and Data Availability

EDM code and data are available at https://github.com/atpham88/US-CE.

G Surplus Available Capacity

We calculate SAC as:

$$SAC_{z,t} = \sum_{i_z \in \mathbb{I}_z} AvailableNonHydroCapacity_{i_z,t} + \tag{32}$$

$$HydropowerGeneration_{z,t} + TransmissionImports_{z,t} \tag{33}$$

$$-TransmissionExports_{z,t} - Demand_{z,t} \tag{34}$$

Hydropower generation and transmission imports and exports are optimized outputs from the EDM. Optimized hydropower generation accounts for temperature-dependent FORs (Table 6) and monthly energy budgets (Section B.3). Available non-hydropower capacity accounts for several factors. In the case of wind and solar, it accounts for wind and solar capacity factors and an assumed 5% FOR (Table 6). For all other non-hydropower plants, it accounts for temperature dependent FORs and, in the case of fossil-based thermal plants (combustion turbines, NGCCs, and coal-fired power plants), thermal deratings (Table 6).